



**Politecnico
di Torino**

INSA

INSTITUT NATIONAL
DES SCIENCES
APPLIQUÉES
CENTRE VAL DE LOIRE

Politecnico di Torino INSA Centre-Val de Loire

Master's Degree in Mechanical Engineering

Simulation model and experimental validation for estimation of fatigue damage due to random vibration

Supervisors:

Cristiana Delprete

Roger Serra

Raffaella Sesana

Candidate:

Luca Campello

December 2021

INDEX

1	<u>INTRODUCTION</u>	4
1.1	FATIGUE FAILURE AND EXISTING ASSESSMENT METHODS	4
1.2	OBJECTIVES AND CONTENTS OF THIS WORK.....	5
2	<u>DYNAMIC SIGNALS</u>	6
2.1	RANDOM SIGNALS	7
2.1.1	STATISTICAL DEFINITION	7
2.1.2	PROBABILITY DISTRIBUTION	9
2.1.3	GAUSSIAN DISTRIBUTION	11
2.1.4	SPECTRUM ANALYSIS & POWER SPECTRAL DENSITY	12
3	<u>FATIGUE</u>	18
3.1	INTRODUCTION.....	18
3.2	PHENOMENOLOGICAL DESCRIPTION	18
3.3	S-N CURVE.....	19
3.4	DAMAGE ASSESSMENT	20
4	<u>METHODS FOR ESTIMATING DAMAGE FROM RANDOM LOADS</u>	22
4.1	TIME-DOMAIN APPROACH	22
4.2	FREQUENCY-DOMAIN APPROACH	23
4.1.1	NARROW BAND APPROXIMATION	24
4.1.2	WIRSCHING-LIGHT METHOD	25
4.1.3	ORTIZ CHEN METHOD	25
4.1.4	DIRLIK METHOD	26
4.1.5	ZHAO-BAKER METHOD	27
4.1.6	LALANNE METHOD.....	28
4.1.7	TOVO-BENASCIUTTI METHOD.....	28
4.1.8	$\alpha_{0.75}$ METHOD	29
4.1.9	LARSEN AND LUTES'S SINGLE MOMENT METHOD	30
4.3	ANALYSIS OF THE METHODS.....	30
5	<u>VIBRATIONS CONCEPTS</u>	33
5.1	SINGLE DEGREE OF FREEDOM.....	33

5.2	MULTIPLE DEGREE OF FREEDOM (MDOF)	35
5.3	FREQUENCY RESPONSE FUNCTION (FRF)	37
5.4	DAMPING	41
5.5	MOTION OF A BEAM	42
6	<u>SIMULATION & EXPERTIMENTAL TESTS</u>	<u>46</u>
6.1	SPECIMEN	47
6.2	EXPERIMENTAL INSTRUMENTS	48
6.2.1	IMPACT HAMMER	48
6.2.2	PIEZOELECTRIC ACCELEROMETER	49
6.2.3	ELECTRODYNAMIC SHAKER	49
6.3	EXPERIMENTAL ACTIVITY	51
6.3.1	EXPERIMENTAL MODAL ANALYSIS	51
6.3.2	STEADY STATE DYNAMIC ANALYSIS – SINE TEST	55
6.3.3	FATIGUE CYCLES LOADS	57
6.4	NUMERICAL SIMULATIONS	60
6.4.1	NUMERICAL MODAL ANALYSIS	60
6.4.2	NUMERICAL STEADY STATE DYNAMIC.....	62
6.4.3	NUMERICAL FATIGUE CYCLES LOADS	65
7	<u>CONCLUSION</u>	<u>68</u>
6	<u>REFERENCE</u>	<u>69</u>

1 INTRODUCTION

1.1 FATIGUE FAILURE AND EXISTING ASSESSMENT METHODS

Many mechanical components are subjected to vibrations. When they are applied, the material is loaded by a certain level of stress, depending on their amplitude and their frequency. If those vibrations endure for long time, a possible structural failure could occur. Such type of failure, called also fatigue failure, happens as a result of accumulated damage. The fatigue failure could happen even if the maximum level of stress is lower than the maximum stress range the material could bear. So, the aim of the designer is to compute the damage of the component subject to vibrations and to predict its useful life to avoid a dangerous failure.

In the case of deterministic and harmonic vibration, estimation fatigue damage methods are widely described in literature. Actually, most vibrations are non-deterministic vibrations or, so called, random vibrations. They are non-deterministic excitations, a type of oscillation whose behavior is non predictable and non-repeatable. The unpredictable behavior of those vibration makes the work of the designer complicated. Fortunately, many methods of predicting the vibration response of mechanical and structural systems to random vibrations have grown rapidly in importance over the last century. The methods allow to compute the fatigue damage both in the time-domain and in the frequency domain. In time domain, Rainflow Cycle Counting and linear damage rule are used, while in the frequency domain several methods are available. Working in frequency domain is an easier way for calculating the damage. In fact, thanks to Fourier transform, it is possible to split a time signal in several harmonic signals, each one with its own frequency. So, it is enough to consider a certain range of frequency for representing several time-signals. In frequency domain the load is described by a function called Power Spectral Density (PSD), which represents the distribution of power into frequency components composing the time-signal.

However, the results of available methods are approximated, and for a reliable estimation of the residual life of the specimen, large and expensive testing campaigns are required. The drawback of the tests are the costs they need for being executed. That is the reason for which the simulation models are a helpful tool nowadays.

1.2 OBJECTIVES AND CONTENTS OF THIS WORK

The purpose of this work is to create a Finite Element Method (FEM)-model whose goal is to predict with a reliable accuracy the fatigue damage and the residual useful life of a AISI 304 specimen loaded with a stress-PSD.

A FEM dynamic model was implemented on ABAQUS to simulate the response of the specimen to a unitary force over a frequency range (Frequency response).

Another FEM model was implemented on nCode, to estimate the damage on the specimen due to a random loading.

Experimental tests have been conducted with the aim of calibrating and validating the simulations with the help of an electrodynamic shaker.

2 DYNAMIC SIGNALS

Signals can be classified according to different criteria. A popular distinction is about a deterministic vibrations and non-deterministic vibrations (Figure 1).

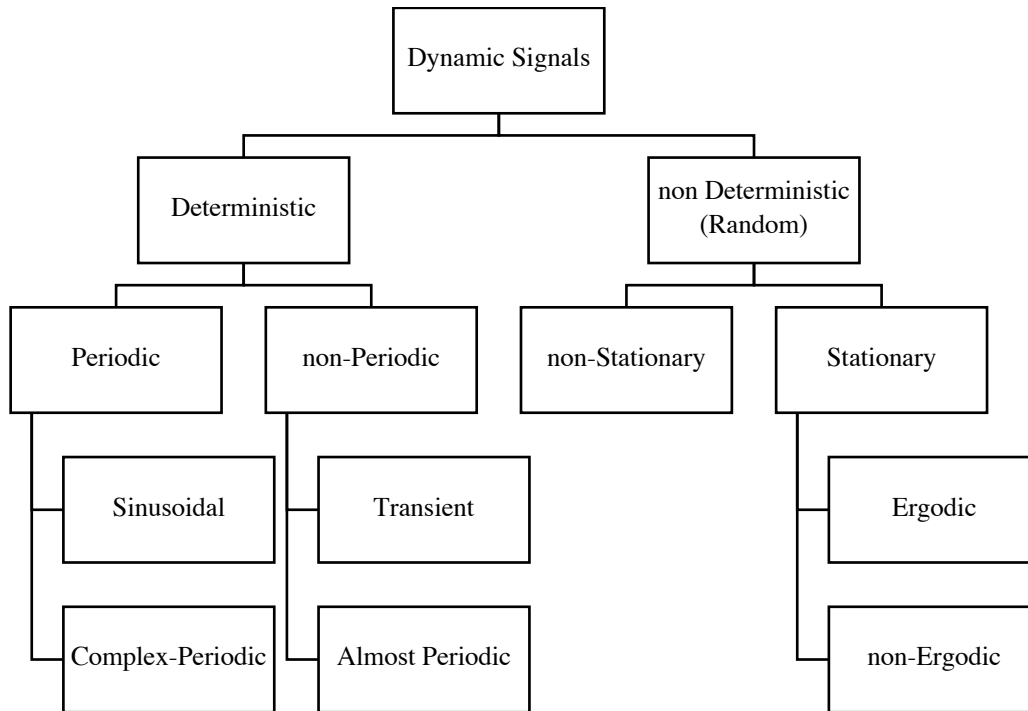


Figure 2.1 Classification of signals [1]

A signal is said to be deterministic if its behaviour is predictable and it could be described by a mathematical expression as $x(t) = A\sin(\omega t + \varphi)$

Non-deterministic signals are a phenomenal whose behaviour is unpredictable and cannot be described by means of mathematical equations due to their lack of repeatability, they are also called Random vibrations.

To verify if a vibration is deterministic or not, it is enough to test if an experiment is able to reproduce the vibration or not. If an experiment generating a defined signal can be replicated with identical results (within the limits of experimental error), then the vibrations can generally be considered deterministic. Instead, if an experiment cannot replicate the results, then the signal must usually be considered random.

Deterministic signals could be classified as either periodic or non-periodic.

Periodic signals are events that repeat in a constant time period, and they can be harmonic or not harmonic. They are sinusoidal when they are described by one frequency (f_1), complex periodic when they are the results of a linear combination of two or more harmonic signals, whose frequencies are multiple of f_1 . [1]

Instead, non-periodic signals can be almost-periodic signals, made by the sum of two or more harmonic whose frequencies are not multiple of fundamental frequency, and transient signals, that can be described by some suitable time-varying function

2.1 RANDOM SIGNALS

Random signals are non-deterministic vibrations (Figure 2.2). They represent a physical phenomenon that cannot be described by meaningful mathematical expression because each observation of the phenomenon will be unique.

They are characterized by many frequency components present over a wide range of frequencies

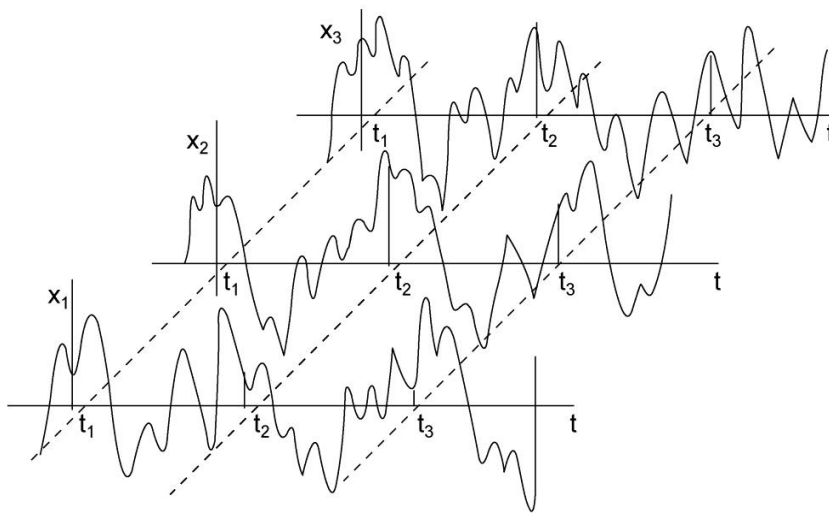


Figure 2.2 Random process [1]

A single time history representing a random phenomenon is called a *sample function*. The entire collection of all possible sample functions that the random phenomenon might have produced is called a *random process*. So, the sample function may be considered as one physical realization of random process. [1]

As said before, lack of repeatability makes difficult to analyze the signal, and to get a suitable way for describing the process is in terms of statistics and probability [1]. In fact, predicting the exact values of the function is not easy, but thanks to statistical and probabilistic analysis, it is possible to predict the probability that a signal with a certain amplitude occurs (acceleration, speed, displacement) [1].

2.1.1 Statistical Definition

A random process consisting in n sample functions $x_k(t)$ ($k = 1, 2, \dots$) is taken into consideration. The mean value of the random process at a certain time instant t_l is obtained by the ratio between the sum

of all the $x_k(t_1)$ values of all the individual sample function and the number of all the n sample functions.

	$\mu_x(t_1) = \lim_{N \rightarrow \infty} \left(\frac{1}{N} \sum_{i=1}^N x_i(t_1) \right) \quad (1)$	
--	---	--

Another relevant statistical parameter is *Autocorrelation function*. It is a correlation between the values of the random process at two different times, computed by taking the ensemble average of the product of instantaneous values at two different times $t=t_1$ and $t=t_2 = t_1 + \tau$

	$R(t_1, t_1 + \tau) = \lim_{N \rightarrow \infty} \left(\frac{1}{N} \sum_{i=1}^N x_i(t_1) x_i(t_1 + \tau) \right). \quad (2)$	
--	--	--

If $\mu(t_1)$ and $R(t_1, t_1 + \tau)$ vary as t_1 varies, the random process is said to be *non-stationary*. In the case where $\mu(t_1)$ and $R(t_1, t_1 + \tau)$ do not vary as time t_1 varies, the random process is said to be *stationary*. For stationary random processes, the mean value is a constant and the auto-correlation function dependent only on the time displacement τ .

$$\mu_x(t_1) = \mu_x = const \quad R(t_1, t_1 + \tau) = R(\tau) = const \quad (3)$$

In most cases, the computation of the mean value and auto-correlation of all ensembles requires a large number of calculations. So, it is possible to describe the properties of a stationary random process by means of a temporal mean value and temporal autocorrelation of a single sample function of the ensemble. For a specific k th sample function, the expression of the temporal mean value and temporal autocorrelation are [1]:

$$\mu_x(k) = \lim_{T \rightarrow \infty} \frac{1}{T} \int_{-\frac{T}{2}}^{\frac{T}{2}} x_k(t) dt \quad (4)$$

$$R_{xx}(\tau, k) = \lim_{T \rightarrow \infty} \frac{1}{T} \int_{-\frac{T}{2}}^{\frac{T}{2}} x_k(t) x_k(t + \tau) dt \quad (5)$$

If the random process is stationary, and $\mu(k)$ and $R(t_1, k)$ don't differ when computed over different sample functions, the random process is said to be *ergodic* [1][2] and so:

$$\mu_x(k) = \mu_x \quad R(t_1, k) = R(\tau) \quad (6)$$

Those expressions mean that all properties of ergodic random processes can be determined by performing time averages over a single sample function [1][2]. Indeed, thanks to this simplification, only stationary ergodic random vibrations will be taken in consideration.

Others useful statistical parameters for characterizing a random variable are:

- mean square value [2]

$$\psi_x^2 = \lim_{T \rightarrow \infty} \frac{1}{T} \int_{-\frac{T}{2}}^{\frac{T}{2}} x^2(t) dt \quad (7)$$

- variance [2]

$$\sigma_x^2 = \lim_{T \rightarrow \infty} \int_{-\frac{T}{2}}^{\frac{T}{2}} [x(t) - \mu_x]^2(t) dt \quad (8)$$

The square of mean square value and variance are called respectively *root mean square* (or *rms*) and *standard deviation*.

From (8) we can obtain

$$\sigma_x^2 = \lim_{T \rightarrow \infty} \int_{-\frac{T}{2}}^{\frac{T}{2}} x^2(t) dt - 2\mu_x \lim_{T \rightarrow \infty} \int_{-\frac{T}{2}}^{\frac{T}{2}} x(t) dt + \mu_x^2 = \psi_x^2 - \mu_x^2 \quad (9)$$

2.1.2 Probability Distribution

The quantities defined earlier are not yet sufficient to completely characterize a random signal. It is also necessary to define a function expressing the probability distribution related to the amplitude of the signal.

For any random value $x(t)$, *probability distribution function* $P(x)$, defined as the probability that $x(t)$ is smaller than a given value x , is written as

$$P(x) = Prob[x(t) \leq x] \quad (10)$$

$$P(-\infty) = 0 \quad (11)$$

$$P(+\infty) = 1 \quad (12)$$

$$P(a) \leq P(b) \text{ se } a \leq b \quad (13)$$

If the $P(x)$ assumes a continuous range of values, a *probability density function* is defined as [1]:

$$p(x) = \lim_{\Delta x \rightarrow 0} \left(\frac{Prob[x < x(k) \leq x + \Delta x]}{\Delta x} \right) = \frac{dP}{dx} \quad (14)$$

It follows that

$$p(x) \geq 0 \quad (15)$$

$$P(x) = \int_{-\infty}^x p(\xi) d\xi \quad (16)$$

$$\int_{-\infty}^{+\infty} p(x) dx = 1 \quad (17)$$

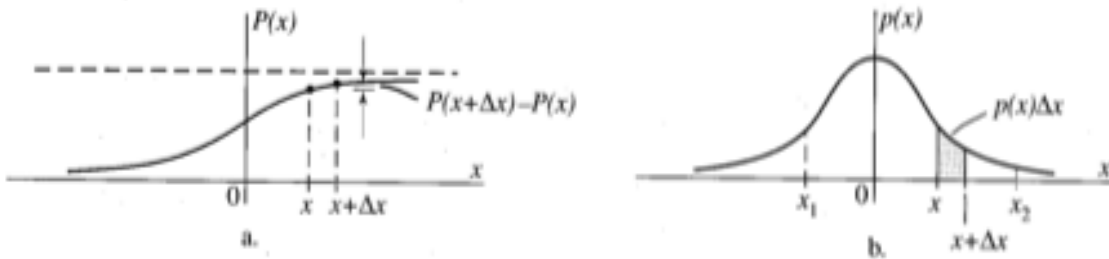


Figure 2.3 a) Probability distribution function; b) Probability density

Finally, it is possible to express the statistical parameters defined in Section 2.1.1 in terms of probability density functions, as shown below.

The *mean value* of $x(k)$ (also called *expected value* or *average value*) is obtained by multiplied each value assumed by $x(k)$ with its probability of occurrence:

$$\mu_x = E[x(k)] = \int_{-\infty}^{+\infty} xp(x)dx \quad (18)$$

Where E[.] is the operator that computes the *expected value* of the variable inside the bracket
Similarly, it is possible to obtain the expected value of *mean square value* and *variance*:

$$\psi_x^2 = E[x^2(k)] = \int_{-\infty}^{+\infty} x^2p(x)dx \quad (19)$$

$$\sigma_x^2 = E[(x(k) - \mu_x)^2] = \int_{-\infty}^{+\infty} (x - \mu_x)^2p(x)dx \quad (20)$$

There are different types of *probability density function*:

- Uniform or rectangular
- Gaussian distribution (or normal distribution)
- Sine Wave
- Rice and Rayleigh distribution

2.1.3 Gaussian Distribution

The Gaussian distribution is probably the most known probability distribution. It is characterized by a probability density function whose expression is:

$$p_G(x) = \frac{1}{\sigma_x\sqrt{2\pi}} e^{-\frac{1}{2}\left(\frac{x-\mu_x}{\sigma_x}\right)^2} \quad (21)$$

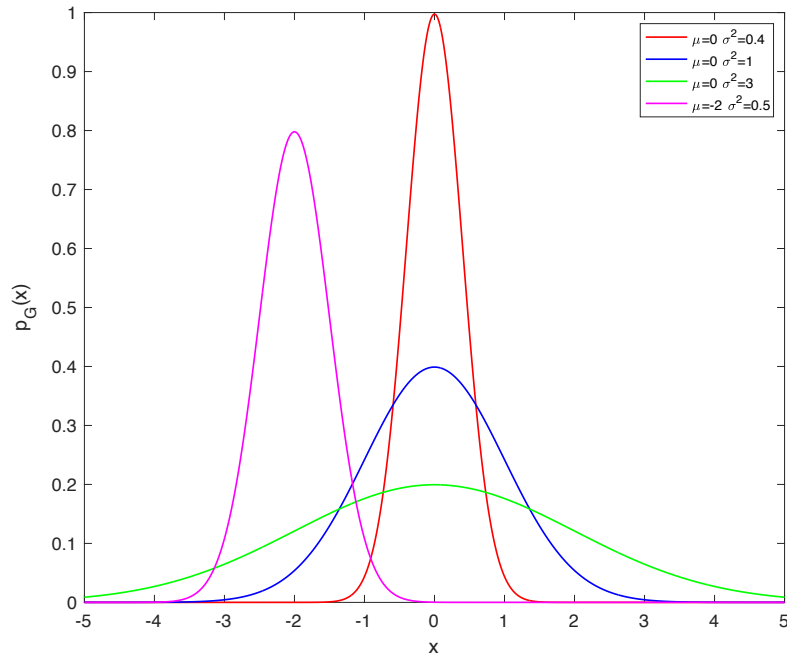


Figure 2.4 Gaussian probability density function

From Figure 2.4 it is possible to understand how the mean value and the variance affects the shape and the position of the curve.

In this research, only Gaussian random signal will be taken into consideration where, for every times instant on an ensemble, the random variables $x(t)$ follow a normal distribution as defined by (21). It can be proved that if the excitation of a linear system is a Gaussian random process, the response is still Gaussian [1].

2.1.4 Spectrum Analysis & Power Spectral density

A random signal is characterized by a series of different frequencies. For this reason, with a non-deterministic signal, it is advisable to pass in frequency domain [2].

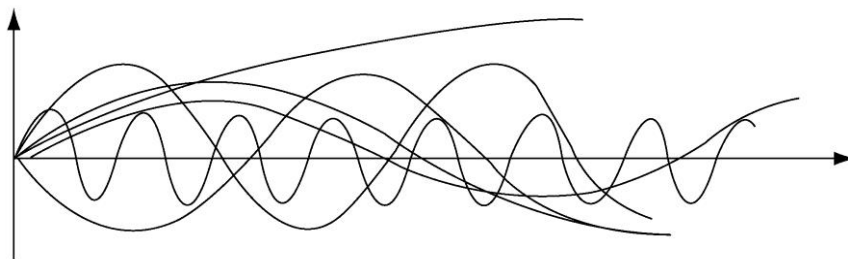


Figure 2.5 Composition of a random signal [2]

It is well known that is possible to write either a periodic signal or a non-periodic signal as the sum of harmonic signals each with its own frequency. The operator transforming time domain functions to frequency domain is the Fast Fourier Transform.

$$F(\omega) = \int_{-\infty}^{+\infty} f(t)e^{-i\omega t} dt \quad (22)$$

The transformation allows to identify and to represent all the frequencies contained in the time-domain random signal. That representation is called *frequency spectrum*.

The autocorrelation provides information concerning characteristic of random signal in time-domain but on the other hand, for gathering information in frequency domain, it is used the *Power Spectral Density (PSD)* [2]. It is defined as the Fourier transform of the autocorrelation function

$$S_{xx}(\omega) \stackrel{\text{def}}{=} \int_{-\infty}^{\infty} R_{xx}(\tau) e^{-i\omega\tau} d\tau \quad (23)$$

which implies that the autocorrelation function can be obtained from the inverse Fourier transform:

$$R_{xx}(\tau) \stackrel{\text{def}}{=} \frac{1}{2\pi} \int_{-\infty}^{\infty} S_{xx}(\omega) e^{-i\omega\tau} d\omega \quad (24)$$

The physical meaning of the PSD can be understood by considering Eq. (3) with $\tau = 0$

	$R(0) = \lim_{T \rightarrow \infty} \frac{1}{T} \int_{-\frac{T}{2}}^{\frac{T}{2}} x_k^2(t) dt = \psi^2 = \frac{1}{2\pi} \int_{-\infty}^{\infty} S_{xx}(\omega) d\omega \quad (25)$	
--	--	--

$S_{xx}(\omega)$ describes how power of a signal or time series is distributed over frequency [2]. Indeed the ψ^2 represent the area under the PSD. PSD provide the information about the shape of random signal. From an engineering point of view, it is very useful an alternative definition of PSD, valid only for positive frequencies, due to the fact that negative frequencies have no physical sense, and usually indicated as $G_{xx}(f)$, $f > 0$ and called *one-sided auto-spectrum* (Figure 2.6) [3]. The relationship between the (23) and $G_{xx}(f)$, is [3]

	$G_{xx}(f) = \begin{cases} 2S_{xx}, & x > 0 \\ 0, & x \leq 0 \end{cases}$	(26)
--	---	------

The correspondence with the stationary correlation function R_{xx} is [2]

	$G_{xx}(f) = 4 \int_0^{\infty} R_{xx}(\tau) \cos 2\pi f \tau \, d\tau$	(27)
--	--	------

Inversely [2]

	$R_{xx}(\tau) = \int_0^{\infty} G_{xx}(f) \cos 2\pi f \tau \, df$	(28)
--	---	------

So, from (28), (25) can be written in this way [3]:

	$R(0) = \psi^2 = \frac{1}{2\pi} \int_0^{\infty} G_{xx}(f) \, df$	(29)
--	--	------

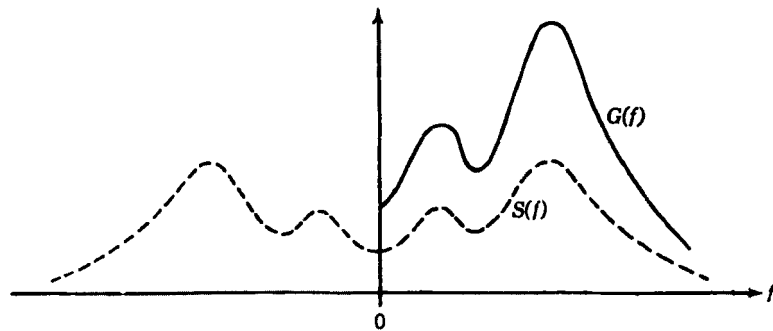


Figure 2.6 definition of one side auto spectrum (G_{xx}) and power spectral density $S(f)$ [1]

From PSD we can also obtain a *spectral moment* [6]:

	$m_i = \int_0^{\infty} \omega^i S_{xx}(\omega) d\omega$	$m = 1, 2, \dots$	(30)
--	---	-------------------	------

	$m_0 = \sigma_X^2, \quad m_2 = \sigma_X^2, \quad m_4 = \sigma_X^4$		(31)
--	--	--	------

Another important classification of signals is related to the frequency range amplitude they are characterized. It is possible to distinguish among a narrowband or a wideband process.

A *narrowband process* is characterized by a sharp peak power spectral density, that is PSD has significant value only in short centered around a frequency value corresponding to the peak. On the other hand, in a *wideband process* the power spectral has significant value in a wide frequency range [2].

At the two extremes of this classification, it could find a sinusoidal sample function whose power spectral density is represented just by two symmetrically placed frequencies, and a sample function whose power spectral density represents all the frequencies equally.

The first is a deterministic function, while the second is known as *white noise*. If the frequency range is infinite, it is called *ideal white noise* (Figure 2.6).

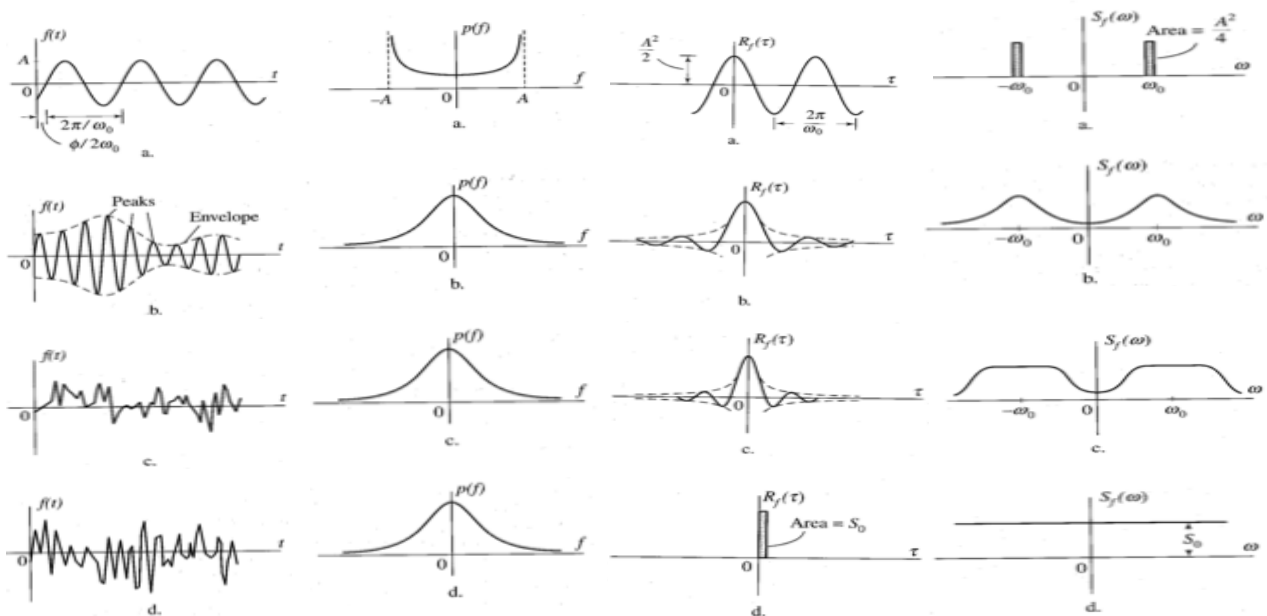


Figure 2.7 Probability density, autocorrelation and PSD function for four sample time histories: (a) sinusoidal, (b) narrowband process, (c) wideband process, (d) white noise. [2]

To characterize a random signal, some other parameters are used:

- Expecting positive zero crossing rate

	$v_0 = \sqrt{\frac{m_2}{m_0}}$	(32)
--	--------------------------------	------

The (32) show the number of crossings level $x(t) = 0$ with positive slopes in a random signal $x(t)$.

- Expecting peak

	$v_p = \sqrt{\frac{m_4}{m_2}}$	(33)
--	--------------------------------	------

It represents the total numbers of positive peak in a random signal.

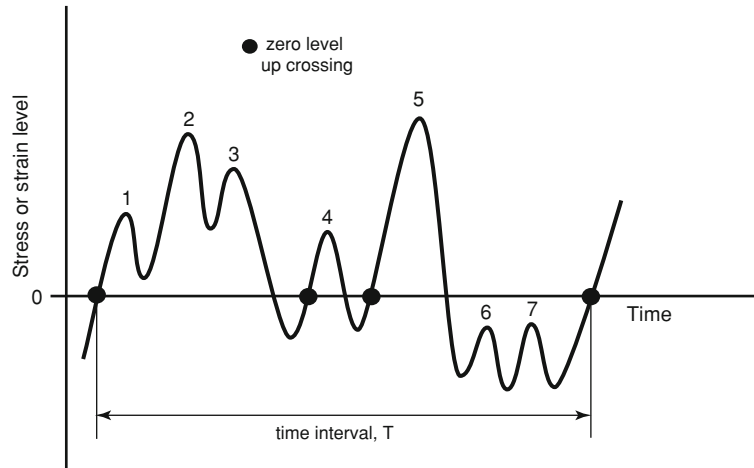


Figure 2.8 Numbers of positive peaks and numbers of level crossings per unit time [4]

If $x(t)$ is a narrow bandwidth random signal, the total expected number of positive peaks is equal to crossing level with positive slope.

Another important function is the *irregularity factor* or *bandwidth parameter* which is given by

$$\alpha_m = \frac{m_i}{\sqrt{m_0 m_{2m}}} \quad (34)$$

With m is an index that can take non-integer value too.

A narrowband process has an irregularity factor close to one and for wideband process it is close to zero.

Rice stated [13] further that for any random stationary Gaussian process, narrowband or wideband, the probability density function of the peaks values is [13]

$$p(x) = \sqrt{\frac{1 - \alpha_2^2}{2\pi m_0}} e^{\left(-\frac{s^2}{2m_0(1-\alpha_2^2)}\right)} + \alpha_2 \frac{S}{M_0} e^{\left(-\frac{s^2}{2m_0}\right)} p_G\left(\frac{\alpha_2 S}{\sqrt{(1 - \alpha_2^2)m_0}}\right) \quad (35)$$

This equation is known as *Rice distribution*.

It is possible to note that for an irregularity factor of 1, the shape is a *Rayleigh distribution* (Figure 2.8)

$$p_R(x) = \frac{x}{\sigma_x^2} e^{-\frac{x^2}{2\sigma_x^2}} \quad (36)$$

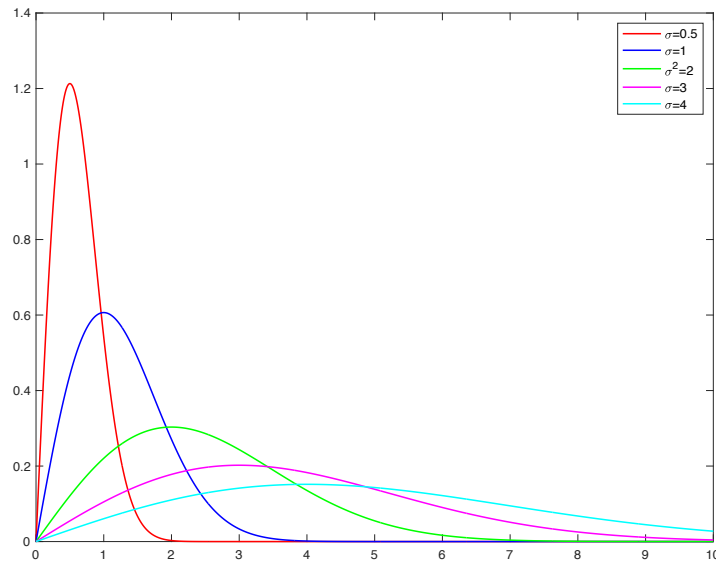


Figure 2.9 Rayleigh probability density function

For an irregularity factor of zero, the shape is a Gaussian distribution

3 FATIGUE

3.1 INTRODUCTION

It has been proved that the repetition of time dependent loads on a material sample strongly reduces the loads which the material can bear; this phenomenon leads to a damage, with the possible consequence of failure. The failure occurs even if the maximum value of the load is lower than both the ultimate tensile strength (UTS) R_m and then the yield strength σ_y of the material. This type of damage is called *fatigue damage* [4].

Several mechanical components are affected by fatigue damage (automobiles on road, wings or fuselage of airplane, rotating shaft...). It has been estimated that fatigue is the cause of approximately 90% of the failure cases [4].

3.2 PHENOMENOLOGICAL DESCRIPTION

The phases of the mechanism related to the fatigue damage are:

- Cracks initiation
- Crack propagation
- Final fracture of the component

In most cases, a fatigue fracture starts from the surface of the component, which presents a certain level of roughness. Because of that, some points on the surface could result as the most loaded and stressed of the component.

This localized high load generates local microplastic deformations which accumulate and initiate small cracks. This initial event can be submicroscopic in size, much less than one tenth of a micron, and contained in a slip line inside a single material grain. The initiation cracks need a large number of cycles to propagate, so that the greatest part of the component's lifetime is spent during this initial stage.

If specimen cyclic loading proceeds, one of the multiple cracks propagates increasing its dimension, while the others are stopped by little obstacles in the material. Due to the stress concentration generated by the crack tip, a plastic zone forms around the crack tip, causing a small crack tip. In this condition the propagation is said to be stable.

The failure occurs when the stress intensity exceeds a critical value known as the *fracture toughness*, the crack achieves a considerable length, and the propagation is said instable throughout the specimen.

The amount of energy required to propagate is higher than the resistance of the material. At the end the specimen has not enough intact surface to bear the load, and it collapses [5].

3.3 S-N CURVE

The *S-N curve*, or *Wohler diagram* is a diagram, obtained by Wohler (1819-1914), which represents a statistical model characterizing the fatigue material performance. In this diagram (Figure 3.1) the numbers of cycle to failure N_f of a material are plotted versus the stress amplitude σ_a (or S) of the load applied to the specimens.

The S-N curves are derived from tests on material samples when a regular sinusoidal stress is applied by a testing machine.

This curve is described by the following equation

$$N^k S = C \tag{37}$$

where C and k are material parameters.

By means of this diagram, it is possible to identify the stress level the material corresponding to statistical failure given a number of cycle or how many cycles it can bear before failure occurs for a given stress level.

The higher is the stress level, the higher is the rate of the crack propagation and the lower are the cycles to failure.

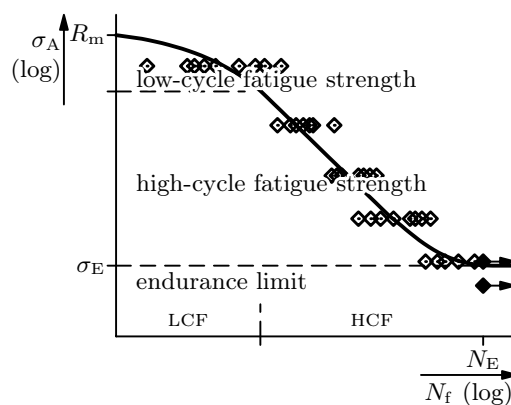


Figure 3.1 Example of S-N curve [5]

If the stress is very low, some material exhibits a *fatigue limit*. In this case, a limiting number of cycles N_E , with the S-N curve being almost horizontal. A specimen which survived N_E cycles is assumed to live infinite life. Frequently, N_E takes values between 2×10^6 and 10^7 , depending on the

material. The stress level corresponding to N_E in the S-N curve is called *endurance limit*, or *fatigue limit* σ_E .

In many materials, there is not horizontal part of the S-N curve. Although the slope of the S-N curve becomes smaller beyond a certain number of cycles, failure can still occur. These materials thus have not fatigue limit [5].

3.4 DAMAGE ASSESSMENT

The S-N diagram plot the useful life of the material at a constant amplitude stress. In actual specimen life, the material is loaded with stress that has variable amplitude, so it results very difficult to estimate the lifetime using diagram.

The most obvious way to estimate specimen and material life is to test the material in laboratory but it takes a large number of tests, and it will be very expensive in term of time and money [5].

Palmgreen and Miner [29] have developed the hypothesis that the fraction of life spent at a given stress amplitude level S_i corresponds to the ratio between the n_i and the allowable cycle N_i at the same stress amplitude S_i . This ratio is a fraction of the critical damage D_{cr} which produces failure by fatigue. The failure is assumed to occur when $D_{cr} = 1$.

Furthermore, Palmgreen and Miner stated that the damage progresses linearly with load repetition. So, the total damage produced by all load contribution at different amplitude is given by [29]:

$$D_{total} = \sum D_i = \sum D_{cr} \frac{n_i}{N_i} \quad (38)$$

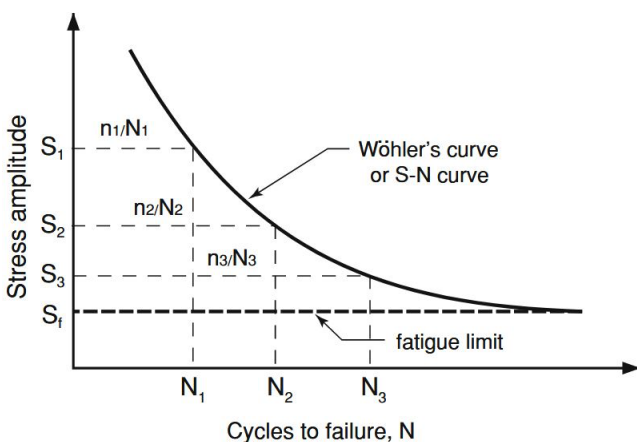


Figure 3.2 Block of three step high load sequence $S_1 >$

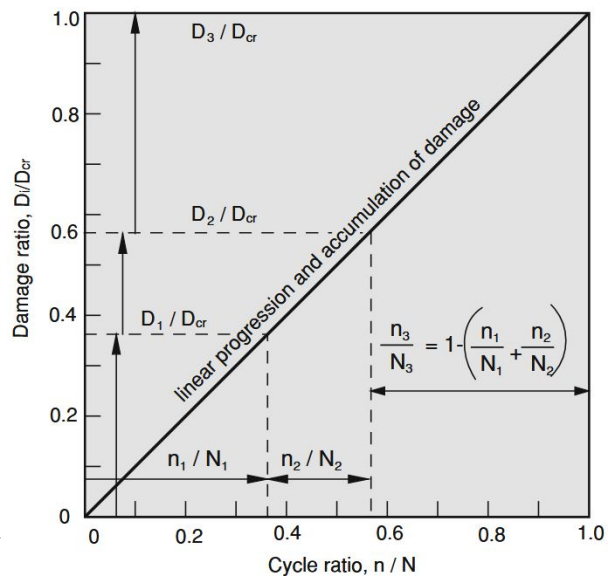


Figure 3.3 Linear damage progression according to Palmgreen-Miner rule [4]

One of the problems with this rule is that the sequence of the load steps is not taken into account. The sequence of loading may influence the fatigue life strongly, an effect neglected in Miner's rule. Even if it is the most used method for its mathematical simplicity, it could be stated that Palmgreen and Miner's rule provide an approximative estimation of fatigue life [5].

4 METHODS FOR ESTIMATING DAMAGE FROM RANDOM LOADS

4.1 TIME-DOMAIN APPROACH

Fatigue analysis for a random loading could be conducted with a time-series approach. For this approach, a cycle counting method to measure the fatigue damage is needed.

Once PDF, the rate of occurrence of counted cycles ν_a and the parameter of $S-N$ curve are known, it possible to calculate the expected fatigue damage, assuming the linear damage rule. Starting from:

$$N \approx C S^{-k} \quad (39)$$

Miner's rule can be rewritten as follows:

$$E[D] \approx \sum_i \frac{n_i}{C S^{-k}} \quad (40)$$

The expected number of cycles at a given stress level per unit time can be written as

$$n_i \approx \nu_p * p(\Delta s) \quad (41)$$

Eq. (40) becomes

$$E[\bar{D}] \approx \nu_p \int_0^{\infty} \left[\frac{p(\Delta s)}{C S^{-k}} \right] ds \quad (42)$$

$$E[\bar{D}] \approx \nu_p C^{-1} \int_0^{\infty} s^k p(\Delta s) * \Delta s \quad (43)$$

Where \bar{D} is the damage per unit time.

The expecting damage after a given time T is obtained by:

$$E[D](T) = T * E[\bar{D}] \quad (44)$$

In Figure 4.1, the logical flow for time series approach is shown.

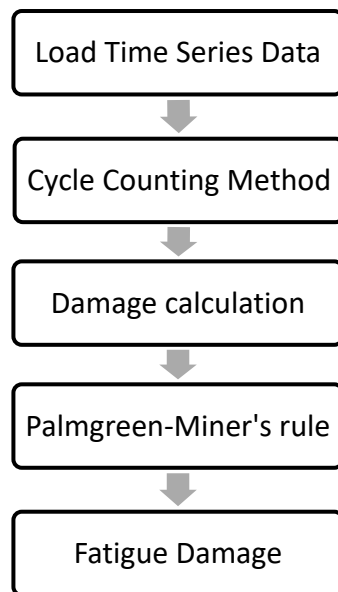


Figure 4.1 Time series approach [13]

Four counting methods are available:

- Peak Counting (PC)
- Level Crossing Counting (LCC)
- Range Counting (RC)
- Rainflow Counting (RFC)

The differences lie the way the peak and the valley are coupled and how the *PDF* is computed [18]. The Rainflow method provides the more accurate results and therefore it is considered as the best cycle counting method [13]. It consists in describing the time load in terms of peak and valley levels or equivalently by its amplitude or mean value [28]. The worst drawback of the method is the long computational time required and a long-time history required to make the results reliable.

4.2 FREQUENCY-DOMAIN APPROACH

The common way to compute the damage is to use spectral methods based on the *PSD* of the load input with the hypothesis that the load is random, ergodic, stationary and Gaussian [11].

The methods will be here analysed are:

- Narrow band approximation (NB)
- Wirsching-Light Method (WL)
- Ortiz-Chen (OC)
- Dirlik method (DK)
- Zhao-Baker Method (ZB)

- Lallane method (LA)
- Tovo-Benasciutti method (TB)
- $\alpha_{0.75}$ method
- Larsen and Luten's single moment method (SM)

Due to the fact that in eq. (43) the only unknown value is $p(\Delta s)$, many solutions suggest different ways to obtain the Probability Density Function (*PDF*) like Dirlik, Zao-Baker and Lallane.

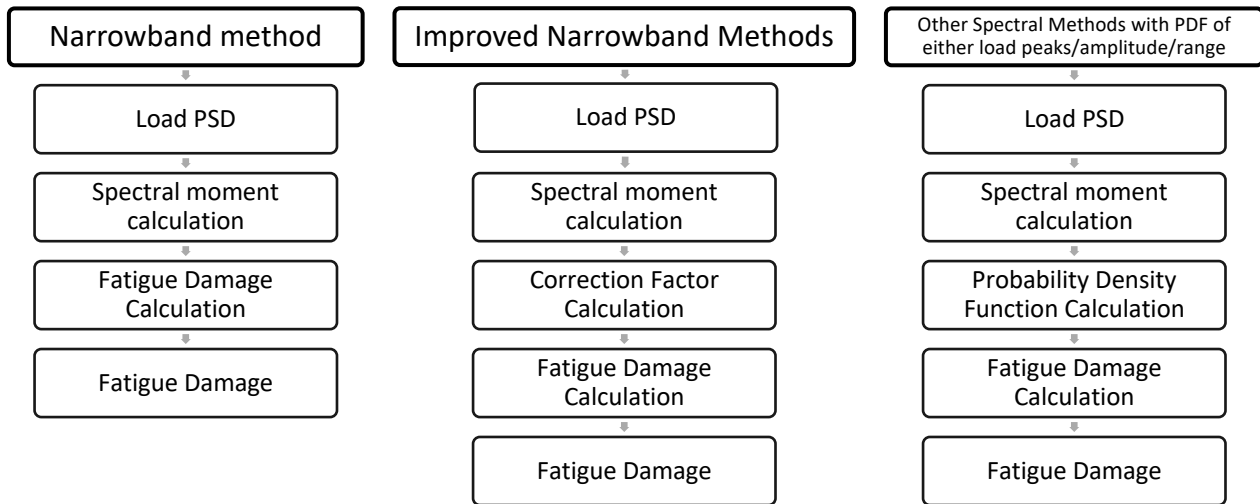


Figure 4.2 Frequency spectral approaches [13]

4.1.1 Narrow Band Approximation

This method is suitable for the case of a narrow-band signal [1]. In this case it has been assumed that every peak is coincident with a cycle, and consequently the amplitude of the probability distribution function can be approximated by Rayleigh distribution [1]:

$$p^{NB}(x) = \frac{S}{\sigma_x^2} e^{-\frac{S^2}{2\sigma_x^2}} \quad (45)$$

Thus, the expression of fatigue damage is defined as:

$$E(\bar{D}^{NB}) = v_p C^{-1} (\sqrt{2m_0})^k \Gamma\left(1 + \frac{k}{2}\right) \quad (46)$$

Where $\Gamma(\cdot)$ is the Euler gamma function, which is defined as:

$$\Gamma(z) = \int_0^{\infty} t^{z-1} e^{-t} dt \quad (47)$$

4.1.2 Wirsching-Light Method

The estimation of the life in a wide band, using the narrow band method, is very conservative, and this brings to underestimate the time to failure [13]. Wirsching and Light proposed [21] to add a parameter to correct the narrow band approximation

$$p(S)^{WL} = \rho^{WL} p(S)^{NB} \quad (48)$$

The ρ_{WL} is the correction factor and its expression is the following:

$$\rho^{WL} = a(k) + [1 - a(k)](1 - \varepsilon)^{b(k)} \quad (49)$$

$$a(k) = 0.926 - 0.033k \quad (50)$$

$$b(k) = 1.587k - 2.323 \quad (51)$$

$$\varepsilon = \sqrt{1 - \alpha_2^2} \quad (52)$$

This method has been investigated and is suitable for k (slope of the S-N curve) values between 3 ÷ 5.

4.1.3 Ortiz Chen Method

Ortiz Chen developed the following correction factor by applying the generalized spectral bandwidth to the Rayleigh distribution [22]

$$p(S)^{OC} = \rho^{OC} p(S)^{NB} \quad (53)$$

The Ortiz Chen correction parameter is expressed as,

$$\rho_k^{OC} = \frac{\beta_k^m}{\alpha_2} \quad (54)$$

With

$$\beta_k = \sqrt{\frac{m_2 m_k}{m_0 m_{k+2}}} \quad (55)$$

4.1.4 Dirlik Method

This is the most famous and known method considered as one of the high accuracy methods [11][12]. It is an empirical formula based on a numerical simulation of the time history. Dirlik proposed [23] an approximation of rainflow cycle counting method by using an exponential distribution and two Rayleigh distribution. The probability distribution is given by:

$$p(S)^{DK} = \frac{1}{2\sqrt{m_0}} \left[\frac{G_1}{Q} e^{\left(-\frac{Z}{Q}\right)} + \frac{G_2 Z}{R^2} e^{-\frac{Z^2}{2R^2}} + G_3 Z e^{-\frac{Z^2}{2}} \right] \quad (56)$$

Where Z is the normalized amplitude and X_m is the mean frequency, as follow:

$$Z = \frac{S}{2\sqrt{m_0}} \quad (57) \quad x_m = \frac{m_1}{m_0} \left(\frac{m_2}{m_4} \right)^{\frac{1}{2}} \quad (58)$$

And the other parameters are defined as:

$$G_1 = \frac{2(x_m - \alpha_2^2)}{1 + \alpha_2^2} \quad (59)$$

$$G_2 = \frac{1 - \alpha_2 + G_1 + G_1^2}{1 - R} \quad (60)$$

$$G_3 = 1 - G_1 - G_2 \quad (61)$$

$$R = \frac{\alpha_2 - x_m - G_1^2}{1 - \alpha_2 - G_1 + G_1^2} \quad (62)$$

$$Q = \frac{1,25(\alpha_2 - G_3 - G_2R)}{G_1} \quad (63)$$

The expression of the fatigue life intensity E has been derived in the form

$$E(D^{DK}) = C^{-1}v_p m_0^{\frac{k}{2}} [G_1 Q^k \Gamma(1+k)] + (\sqrt{2})^k \Gamma\left(1 + \frac{k}{2}\right) (G_2 |R|^k + G_3) \quad (64)$$

One of the problems of this solution is that “even if providing fairly precise damage predictions (as already shown by data from the literature has no theoretical framework (i.e. it represents a completely approximate formula)” [11]

4.1.5 Zhao-Baker Method

W. Zhao and M. Baker propose [24] an expression of PDF obtained by a linear combination of Weibull PDF and Rayleigh PDF, corresponding to small stress range and to large stress range respectively. The model has been validated by comparing the PDF obtained from the model with that obtained by simulation and rainflow counting for a wide range of stress spectra.

The expression is as follows

$$p(S)^{ZB} = \underbrace{w\alpha\beta\left(\frac{S}{\sigma_{RMS}}\right)^{\beta-1}e^{-\alpha\left(\frac{S}{\sigma_{RMS}}\right)^\beta}}_{Weibull} + \underbrace{(1-w)\left(\frac{S}{\sigma_{RMS}}\right)e^{\left(\frac{-S}{\sigma_{RMS}}\right)^2}}_{Rayleigh} \quad (65)$$

Where w is the weighting factor defined as

$$0 < w = \frac{1 - \alpha_2}{1 - \sqrt{\frac{2}{\pi}} \Gamma\left(1 + \frac{1}{b}\right) \alpha_2^{-\frac{1}{\beta}}} < 1 \quad (66)$$

And α e β are the Weibull parameters

$$\alpha = 8 - 7\alpha_2 \quad (67)$$

$$\beta = \begin{cases} -1.1 & \alpha < 0.9 \\ 1.1 + 9(\alpha_2 - 0.9) & \alpha \geq 0.9 \end{cases} \quad (68)$$

When $k=3$, the correction factor has a stronger correlation to $\alpha_{0.75}$ rather than α . So, Zhao and Baker offered an enhanced method, where:

$$\alpha = d^{-\beta} \quad (69)$$

With d calculated as a root of

$$\Gamma\left(1 + \frac{3}{\beta}\right)(1 - \alpha_2)d^3 + 3\Gamma\left(1 + \frac{1}{\beta}\right)(\rho_{ZB}\alpha_2 - 1)d + 3\sqrt{\frac{\pi}{2}}\alpha_2(1 - \rho_{ZB}) = 0 \quad (70)$$

And the correction factor is determined by

$$\rho_{ZB|k=3} = \begin{cases} -0.4154 + 1.392\alpha_{0.75} & \alpha_{0.75} \geq 0.5 \\ 0.28 & \alpha_{0.75} < 0.5 \end{cases} \quad (71)$$

The fatigue damage intensity is calculated as follows:

$$E(D^{ZB1/ZB2}) = \frac{v_p}{C} \sigma_X^k \left[wa^{-\frac{k}{\beta}} \Gamma\left(1 + \frac{k}{\beta}\right) + (1 - w)2^{\frac{k}{2}} \Gamma\left(1 + \frac{k}{2}\right) \right] \quad (72)$$

4.1.6 Lalanne Method

Lalanne proposed [25] to add as PDF into eq (43), for calculating the expected fatigue damage, the same of that used by Rice

$$p(S)^{LA} = \sqrt{\frac{1 - \alpha_2^2}{2\pi m_0}} e^{\left(-\frac{s^2}{2m_0(1 - \alpha_2^2)}\right)} + \alpha_2 \frac{S}{M_0} e^{\left(-\frac{s^2}{2m_0}\right)} p_G\left(\frac{\alpha_2 S}{\sqrt{(1 - \alpha_2^2)m_0}}\right) \quad (73)$$

4.1.7 Tovo-Benasciutti Method

Tovo-Benasciutti derived an expression for estimating the expected rainflow fatigue damage [11, 26]. They based on the hypothesis that the damage estimation, from the equivalent loading history

obtained by Rainflow counting method \bar{D}^{RFC} , is lower than or equal to the Narrow band expected damage \bar{D}^{NB} and higher than or equal to Range counting method \bar{D}^{RC} .

$$\bar{D}^{RC} \leq \bar{D}^{RFC} \leq \bar{D}^{NB} \quad (74)$$

where

$$\bar{D}^{RC} = \bar{D}^{NB} \alpha_2^{k-1} \quad (75)$$

Thus, the solution is proposed as a weighted linear combination of these two bounds as follows

$$E(\bar{D}^{TB}) = b\bar{D}^{NB} + (1 - b)\bar{D}^{RC} \quad (76)$$

Two different ways to determine the factor b are suggested:

$$b^{TB1} = \min \left\{ \frac{\alpha_1 - \alpha_2}{1 - \alpha_1}, 1 \right\} \quad (77)$$

$$b^{TB2} = (\alpha_1 \alpha_2) \frac{[1.112(1 + \alpha_1 \alpha_2 - (\alpha_1 + \alpha_2))e^{2.11\alpha_2} + (\alpha_1 + \alpha_2)]}{(\alpha_2 - 1)^2} \quad (78)$$

The b coefficient requires four spectral moments: m_0, m_1, m_2 and m_4 , which in combination form two parameters, α_1 and α_2 .

4.1.8 $\alpha_{0.75}$ Method

It is further method proposed by Benasciutti and Tovo [11, 26]. It states that the correction factor depends on spectral parameters $\alpha_{0.75}$.

$$\rho^\alpha = \alpha_{0.75}^2 \quad (79)$$

$$E(\bar{D}^\alpha) = \rho^\alpha E(\bar{D}^{NB}) \quad (80)$$

4.1.9 Larsen and Lutes's single moment Method

The Larsen and Lutes' single moment method was developed after extensive examination of simulation data and rainflow analysis [27]

$$\rho^{SM} = \frac{\left(\frac{m_i}{m_0}\right)^{m/2}}{v_0} \quad (81)$$

$$i = \frac{2.0}{k} \quad (82)$$

Hence the expected damage is calculated estimated as follows

$$E(\bar{D})^{SM} = \frac{(M_k)^{m/2} T(\sqrt{2})^k}{C} \Gamma\left(\frac{1}{2}k + 1\right) \quad (83)$$

The damage estimation needs the calculation of only a single moment, m_k .

4.3 ANALYSIS OF THE METHODS

Matjaz Mrsnik, Janko Slavic, Miha Boltezar [12] compared the spectral methods to the life estimated with the time series approach, using a combination of rainflow cycle counting and Palmgren and Miner's rule. Two methods were not considered: the method proposed by Ortiz and Chen and the Single-Moment method. The analysis has been conducted assuming, for experimental tests, accelerated vibration tests obtained with an electrodynamic shaker. The acceleration profile was 20m/s^2 in a frequency range from 10 to 1000 Hz. In this range, five different *PSD* were applied. As regards material properties, three different value of *S-N* slope k (3.324, 7.3, 11.76) were used.

The fatigue-life estimations for the frequency-domain methods were compared to the life estimations in the time domain using a combination of the rainflow counting and the Palmgren-Miner hypothesis, which, in this study, is assumed to be the reference value.

The obtained results have showed that Tovo-Benasciutti give the better damage estimation, followed by the improved Zhao-Baker and Dirlik methods. Overall, the results gathered with Dirlik, Zhao-Baker and Tovo-Benasciutti methods are “*all very consistent when the material fatigue parameter k*

is relatively low ($k \approx 3$)” [12] but when the slope became steeper, the difference from the reference estimation increases.

Curtis and Irvine conducted the same analysis [15] considering in this case Ortiz and Chen and the Single-Moment method. According to their analysis the more reliable methods are: Dirlik method, Tovo-Benasciutti method, Ortiz Chen, Single Moment and $\alpha_{0.75}$ method (Figure 4.3 and Figure 4.4). The Dirlik and Tovo-Benasciutti methods underestimate or approach from lower values to the rainflow damage estimation, with the Dirlik method being somewhat more accurate. Instead, Ortiz-Chen and $\alpha_{0.75}$ method overestimate the results. As reported in [15], also in this investigation the increase of the value of k makes the error bigger.

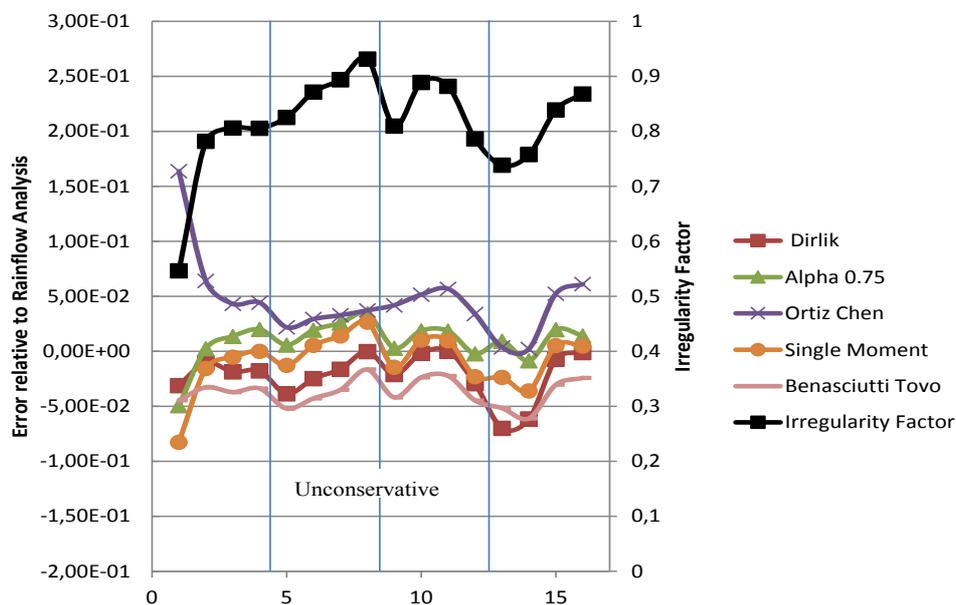


Figure 4.3 Relative error of best spectral methods compared to rainflow analysis

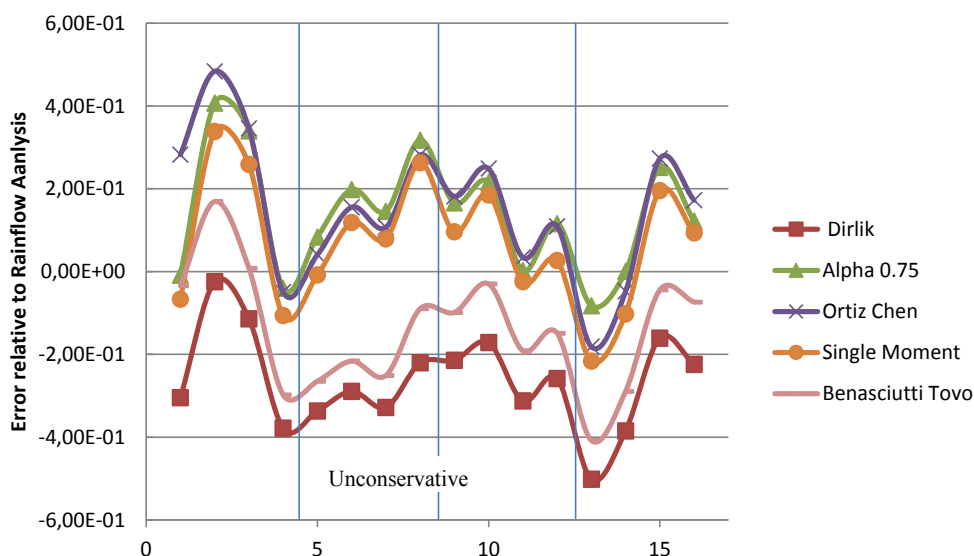


Figure 4.4 Relative error of best spectral methods compared to rainflow analysis for $m=11.76$ [15]

Quigley, Lee and Wang [13] compared the methods with Rainflow method in term of standard deviation and the average error (Figure 4.5 and 4.6). The experiments were conducted using Seventy power spectrum densities with varied amplitude, shape, and irregularity factors from Dirlik's dissertation are used to study the accuracies of these methods. The results showed the OC, $\alpha .75$, SM, Dk and BT methods to be significantly more accurate than the others. These five methods have a tendency for the error variation to increase as the *S-N slope exponent k* increases. In Figure 4.5 and 4.6, the *S-N slope exponent k* is expressed with the symbol *m*

m	NB	WL	OC	BT	SM	$\alpha_{.75}$	ZB	LaL	Dirlik
3	0.27	0.21	0.06	0.02	0.05	0.04	0.21	0.41	0.04
4	0.32	0.24	0.08	0.03	0.08	0.06	0.26	0.41	0.06
5	0.33	0.25	0.11	0.06	0.10	0.09	0.28	0.39	0.08
6	0.33	0.24	0.14	0.08	0.12	0.12	0.29	0.37	0.11
7	0.32	0.22	0.16	0.09	0.14	0.14	0.29	0.36	0.12
8	0.32	0.21	0.18	0.11	0.16	0.16	0.30	0.34	0.14
9	0.31	0.20	0.20	0.12	0.18	0.18	0.31	0.33	0.15
10	0.31	0.18	0.22	0.14	0.19	0.19	0.31	0.33	0.17
11	0.31	0.17	0.24	0.15	0.20	0.20	0.33	0.32	0.18
12	0.30	0.16	0.25	0.16	0.22	0.22	0.35	0.32	0.19

Figure 4.5 Standard deviation versus *S-N slope exponent m* [13]

m	NB	WL	OC	BT	SM	$\alpha_{.75}$	ZB	LaL	Dirlik
3	0.36	0.14	0.00	-0.04	-0.05	-0.03	0.12	0.47	-0.06
4	0.43	0.15	0.00	-0.09	-0.07	0.01	0.16	0.51	-0.09
5	0.47	0.12	-0.01	-0.13	-0.09	0.04	0.19	0.53	-0.12
6	0.48	0.08	-0.03	-0.17	-0.10	0.05	0.20	0.53	-0.14
7	0.49	0.04	-0.04	-0.20	-0.11	0.06	0.20	0.53	-0.16
8	0.49	-0.01	-0.04	-0.22	-0.12	0.06	0.21	0.53	-0.17
9	0.49	-0.06	-0.05	-0.24	-0.13	0.07	0.21	0.52	-0.18
10	0.49	-0.11	-0.05	-0.25	-0.13	0.07	0.22	0.52	-0.19
11	0.49	-0.16	-0.05	-0.27	-0.13	0.08	0.23	0.52	-0.19
12	0.50	-0.21	-0.05	-0.27	-0.14	0.08	0.25	0.52	-0.19

Figure 4.6 Average error versus *S-N slope exponent m* [13]

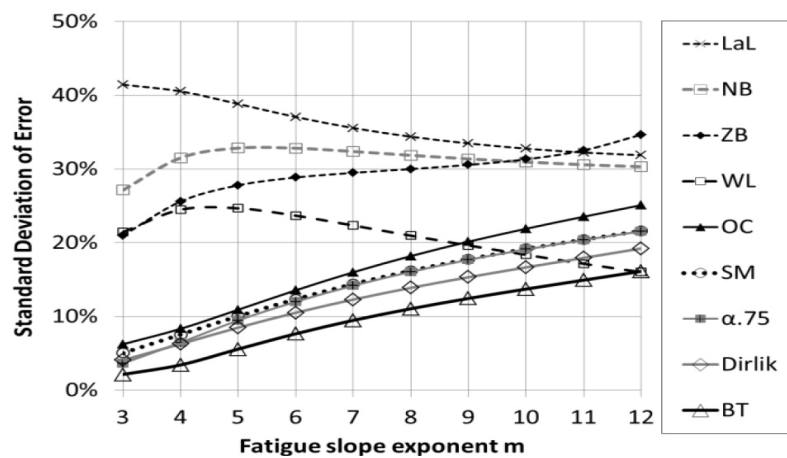


Figure 4.7 Standard deviation of error versus fatigue slope exponent *m* [13]

5 VIBRATIONS CONCEPTS

In this research, it will be taken into consideration a linear system, that is, “a system where the time depended variable $x(t)$ and all its time derivative appear in the equation of motion to the first power or zero power only” [2]

5.1 SINGLE DEGREE OF FREEDOM

A single degree of freedom system (SDOF) is a system where the motion of all its parts at any instant of time is completely defined with just one coordinate, or variable [3].

A linear SDOF system consists in a mass m , linear viscous damper c , linear springer k and excitation force $f(t)$. Let x be the coordinate that locates mass m , the equation of the motion of the system is:

$$m\ddot{x} + c\dot{x} + kx = f(t) \quad (84)$$

if $f(t) = 0$ the vibration is said to be a *free vibration*, otherwise if $f(t) \neq 0$ the vibration is called *forced vibration* [3]. The solution $x(t)$ (84) changes in function of the value of $f(t)$.

If $f(t) = 0$, the response of the system $x(t)$ is [3]:

	$x_c = e^{-\zeta\omega_n t} [A \cos(\omega_d t) + B \sin(\omega_d t)]$	(85)
--	--	------

Where

	$\omega_n = \sqrt{\frac{k}{m}}$	(86)
--	---------------------------------	------

is *natural frequency*

	$\zeta = \frac{c}{c_{cr}} = \frac{c}{\sqrt{mk}}$	(87)
--	--	------

is defined *damping ratio*, and

	$\omega_d = \omega_n \sqrt{1 - \zeta^2}$	(88)
--	--	------

is *damped frequency* [3].

A e B are constant, and they are derived from the value of \dot{x} and x at the time instant $t=0$.

If $f(t)$ is a constant value f_0 the solution is the sum of the free vibration response (transient solution) and force vibration response (steady-state solution) [3]:

	$x(t) = \frac{f_0}{k} + e^{-\zeta\omega_n t} [A \cos(\omega_d t) + B \sin(\omega_d t)]$	(89)
--	---	------

Instead, if $f(t)$ is a harmonic excitation, only the steady-state solution could be considered, because the transient solution has a significant effect just for a limited period of time [3][7].

Therefore, for a harmonic force, it can be stated that [3]

	$f(t) = F_0 e^{-i\omega t}$	(90)
--	-----------------------------	------

where ω is the *excitation frequency* or *driving frequency*, and that the solution of (84) is

	$x(t) = x_0 e^{-i\omega t}$	(91)
--	-----------------------------	------

Substitution of (90) and (91) in (84) gives:

	$(k - \omega^2 m + i\omega c)x_0 = F_0$	(92)
--	---	------

So

	$x(t) = \frac{F_0}{(k - \omega^2 m + i\omega c)} e^{-i\omega t}$	(93)
--	--	------

The equation (93) could be written in this way

$$x_0 = \frac{F_0}{(1 - r^2) + i(2\zeta r)} \tag{94}$$

With

$$r = \frac{\omega}{\omega_n} \quad (95)$$

5.2 MULTIPLE DEGREE OF FREEDOM (MDOF)

In chapter 4.2. a single degree of freedom has been introduced to describe a structure's dynamic behaviour in the simplest possible terms. However, most of real mechanical systems and structures are continuous systems that have infinite degree of freedom and so it is not suitable assuming a single degree of freedom for a complete description. Therefore, their behaviour is described by more than one coordinate for any instant time. The number of N finite number of degrees of freedom used for conducting the analysis must be enough to ensure a reliable result [8].

The equation (36) became:

	$[M]\{\ddot{x}\} + [C]\{\dot{x}\} + [K]\{x\} = \{f\}$	(96)
--	---	------

Where $[M]$, $[C]$, $[K]$ are $N \times N$ mass, damping and stiffness symmetric matrices respectively. The $N \times 1$ column vector $\{\ddot{x}\}$, $\{\dot{x}\}$, $\{x\}$ and are the acceleration, velocity and displacement respectively and $\{f\}$ is the $N \times 1$ vector of the external excitation forces [8].

The solution of the equation (96) is obtained by a mathematical procedure called *modal analysis*, where it is possible to find the natural frequency and modes of vibration of the system.

To determine the natural frequencies, it is needed to start from the undamped system and free vibration system and to solve the eigenvalue problem.

It starts from [3][7][8]:

$$[M]\{\ddot{x}\} + [K]\{x\} = 0 \quad (97)$$

Assuming the solution to be harmonic [3][7][8]

$$\{x(t)\} = \{X\} \sin(\omega t + \varphi) \quad (98)$$

Eq (97) can be written [3][7][8]:

$$[[K] - \omega^2[M]]\{X\} = 0 \quad (99)$$

One of the solutions of the system is the trivial solution $\{X\} = 0$ but there is no interest in that because it means that there is no motion at all. As consequence, to have non-trivial solution,

$$\det[[K] - \omega^2[M]] = 0 \quad (100)$$

must be satisfied.

$\det[.]$ stands for *determinant* and (100) is an algebraic equation, known as the *characteristic equation* which concede N possible positive and real solutions $\omega_1^2, \omega_2^2, \dots, \omega_N^2$ called *eigenvalue* of (51). The value $\omega_1, \omega_2, \dots, \omega_N$ are the undamped natural frequencies of our system [8].

Substituting each natural frequency value in (100) and solving each of the resulting sets of equations, N possible vector solutions $\{\psi_r\}$ (with $r=1 \dots N$) called *eigenvector* or *mode shapes* are found. At the end, two matrices are obtained: *eigenvalue matrix*, defined as

$$[\omega_r^2] = \begin{pmatrix} \omega_1^2 & \dots & 0 \\ \vdots & \ddots & \vdots \\ 0 & \dots & \omega_N^2 \end{pmatrix} \quad (101)$$

And *eigenvector matrix*

$$[\Psi] = [\{\psi_1\}, \{\psi_2\}, \dots, \{\psi_N\}] \quad (102)$$

The physical meaning consists in the description of the synchronous motion of the system. It vibrates freely at N particular frequency values ω_r with a particular shape defined by the $\{\psi_r\}$. For each ω_r is associated a unique $\{\psi_r\}$. Each pair of ω_r and $\{\psi_r\}$ is known as a mode of vibration of the system [3][7]. An important property of the modes shapes is orthogonality properties that make both mass and stiffness matrix a diagonal matrix. In fact, It can be demonstrated that [3][7][8]:

	$[\Psi]^T[M][\Psi] = \begin{bmatrix} m_1 & \dots & 0 \\ \vdots & \ddots & \vdots \\ 0 & \dots & m_r \end{bmatrix} = \text{diag}(m_r)$	(103)
	$[\Psi]^T[K][\Psi] = \begin{bmatrix} k_1 & \dots & 0 \\ \vdots & \ddots & \vdots \\ 0 & \dots & k_r \end{bmatrix} = \text{diag}(k_r)$	(104)

(56) is called *modal mass matrix* and (57) is called *modal stiffness matrix*. These properties of the matrix are used to find the free vibration solution.

It is possible to define the *direct modal transformation*

$$\{x(t)\} = [\Psi]\{\eta(t)\} = \sum_i^N \{\psi_i\} \eta_i(t) \quad (105)$$

$\{\eta(t)\}$ is the vector of the modal displacement

The vector $\{x(t)\}$ is expressed as the sum of the response of each modal shapes (*superposition of the normal modes responses*). Therefore, eq. (97) can be written in this way:

	$[M][\Psi]\{\ddot{\eta}(t)\} + [K][\Psi]\{\eta(t)\} = 0$	(106)
--	--	-------

Considering (86), (103) and (104), it can be simplified [3], [7], [8].

	$\{\ddot{\eta}(t)\} + [\omega_i^2]\{\eta(t)\} = 0$	(107)
--	--	-------

Thus, through a simple transformation, the MDOF system has been transformed into N independent SDOF systems where each equation of motion depends solely on a coordinate η_i [3][7][8].

For solving (96), the procedure is the same of (105). Thus, (97) became

	$[M][\Psi]\{\ddot{\eta}(t)\} + [C][\Psi]\{\dot{\eta}(t)\} + [K][\Psi]\{\eta(t)\} = \{f(t)\}$	(108)
--	--	-------

And the solution is given by

$$\{X_0\} = \sum_{r=1}^N \frac{\{\psi_r\}^T \{F_0\} \{\psi_r\}}{k_r - \omega^2 m_r + i \omega c_r} \quad (109)$$

5.3 FREQUENCY RESPONSE FUNCTION (FRF)

Eq (94) could be expressed in a different way, as well:

	$x_0 = H(\omega)F(\omega)$	(110)
--	----------------------------	-------

$H(\omega)$ is called the frequency response function. It is a transfer function, expressed in the frequency-domain. It expresses the structural response to an applied force as a function of frequency (Figure 5.1) [17]. The system will respond with a harmonic vibration with the same frequency ω but with an amplitude and phase shift, with respect to the force determined by the magnitude and the phase of the complex quantity $x(\omega)$.

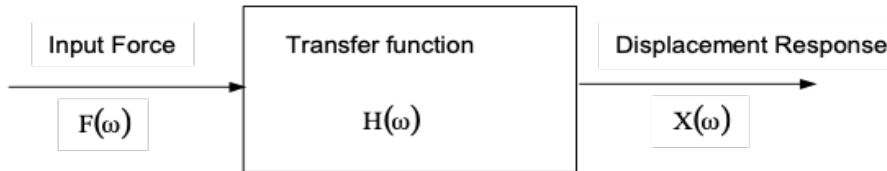


Figure 5.1 Frequency response function chart

The frequency response is a complex number with real and imaginary part:

$$H(\omega) = \frac{1}{\underbrace{k - \omega^2}_{\text{real}} + \underbrace{ic\omega}_{\text{imaginary}}} \quad (111)$$

The response could be given in term of displacement, velocity and acceleration.

If the response is in term of displacement, the FRF is called *receptance*,

	$\frac{X(\omega)}{F(\omega)} = \frac{1}{(\omega_n^2 - \omega^2) + j2\xi_n\omega\omega_n} \quad (112)$	
--	---	--

if it is in term of velocity, FRF is called *mobility*

$$\frac{\dot{X}(\omega)}{F(\omega)} = \frac{j\omega}{(\omega_n^2 - \omega^2) + j2\xi_n\omega\omega_n} \quad (113)$$

while in term of acceleration, FRF is called *inertance*

$$\frac{\ddot{X}(\omega)}{F(\omega)} = \frac{\omega^2}{(\omega_n^2 - \omega^2) + j2\xi_n\omega\omega_n} \quad (114)$$

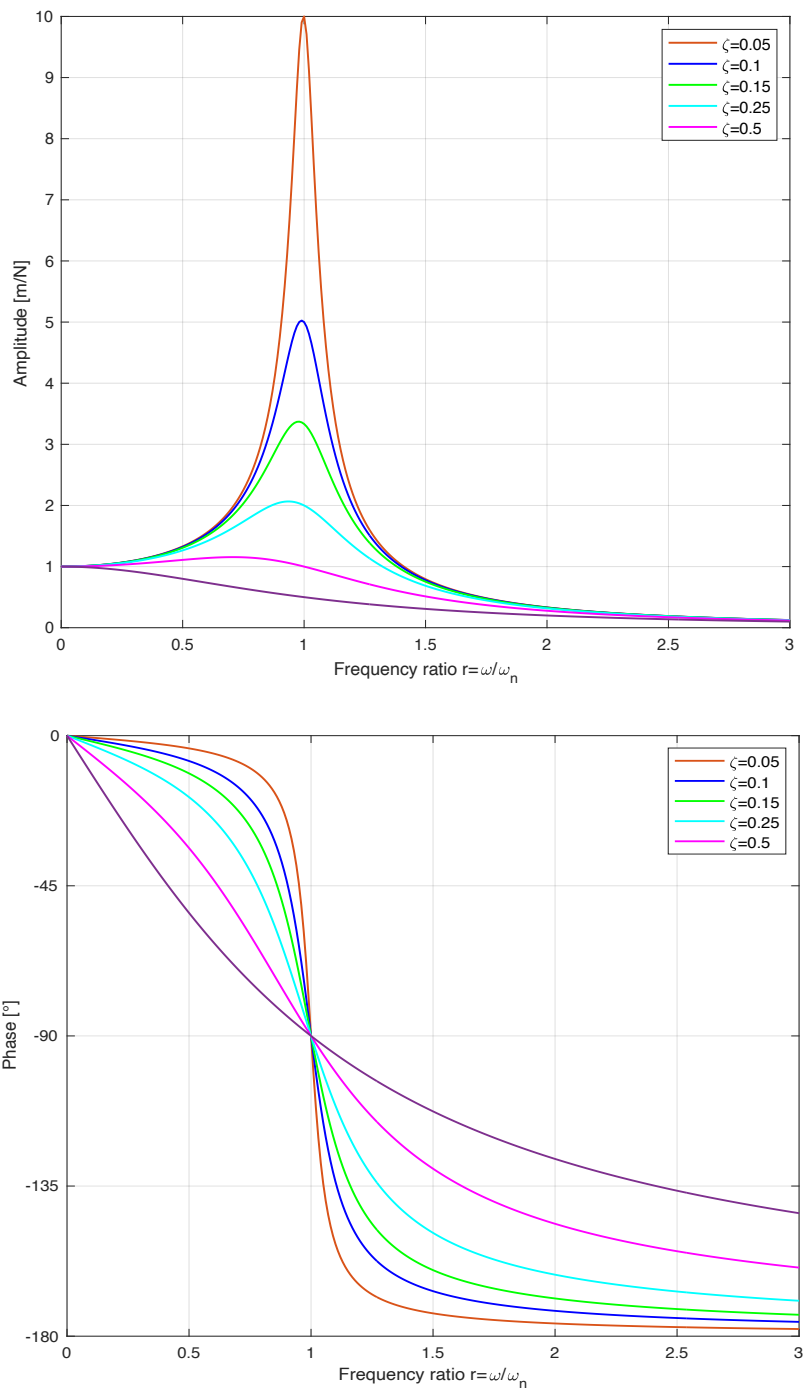


Figure 5.2. Amplitude and phase of the harmonic vibration response

In Figure 5.2, it is shown the displacement of the structure. It is possible to note that when $r \approx 1$ the amplitude of the function reaches the maximum point. That point means that the frequency of force excitation ω coincides with the natural frequency of the system ω_n and a condition, known as *resonance*, occurs. The amplitude of the resonance depends on the damping on the structure. In these conditions, the system has large and dangerous oscillations and the risk of the failure is high.

In MDOF, the expression of the receptance is given by:

$$H(\omega)_{jk} = \frac{X_j(\omega)}{F_k(\omega)} = \sum_{r=1}^N \frac{\{\psi_{jr}\}^T \{\psi_{kr}\}}{k_r + \omega^2 m_r + i c_r \omega} \quad (115)$$

(115) shows that receptance is a matrix whose element is a two-point relation: R_{jk} describe the relation between the motion response and the excitation force at a coordinates j and k , respectively.

In contrast to the SDOF, the plot for MDOF show multiple peaks because there are more than one receptance (Figure 5.3).

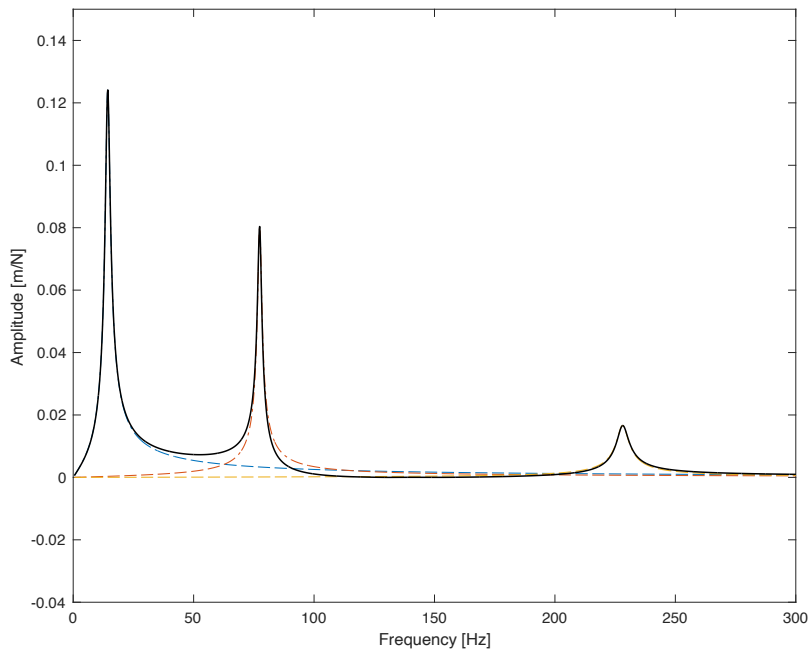


Table 5.3 Amplitude of the response of a MDOF system

As it said in chapter 2, the information concerning a random process can be obtain by Power Spectral density. In the case the input of random vibration is given in term of PSD, the expression of the response is as follow

$$S_{YY} = H(\omega)^2 * S_{XX} \quad (116)$$

Where S_{XX} is the PSD in input and S_{YY} is the PSD in output. PSD dimensionally is: $\frac{unit^2}{Hz}$. The term unit depends on which physical parameter is evaluated. Following the different units of measure for the different parameters are listed

- for Acceleration: $(m/s^2)^2/Hz$ or g^2/Hz
- for Velocity: $(m/s)^2/Hz$
- for Displacement: $(m)^2/Hz$

- for Force: $(N)^2/Hz$
- for Stress: $(MPa)^2/Hz$

5.4 DAMPING

In mechanical vibration, damping is an intrinsic characteristic of the material. It is the cause of energy loss each time it is transformed from potential to kinetic energy and back, causing a decrease in time of the amplitude of free oscillations. The mechanism of the damping is complex to described due to his lack of linearities but approximately his effect is proportional to the speed of the vibrations [9]. There are many different type of damping (viscous, coulomb..). The damping explained here is called: *structural or hysteretical damping*.

Structural damping is an internal friction, that many materials exhibit when subjected to cyclic loading. This energy losses per cycle of stress is equal to the area inside the hysteresis loop (Figure 5.3)

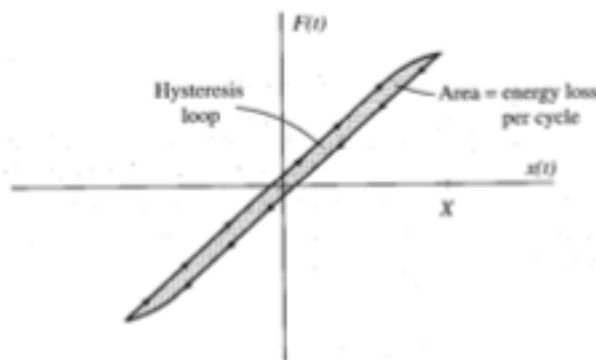


Figure 5.4 Hysteresis loop

In general, this type of damping doesn't lead to an easy modelling. However, it is possible to describe structural damping as viscous damping, making the analysis easier.

Experiments performed show that the energy loss per cycle by a structural damping is proportional to the square of the amplitude [2][3]

$$E = \alpha A^2 \quad (117)$$

Where α is a constant independent of the frequency of the harmonic oscillation.

The energy dissipated by a viscous damping is

$$E = c\pi\omega A^2 \quad (118)$$

Where it follows that the energy dissipated per cycle is directly proportional to the viscous damping coefficient c [2].

Comparing eqs (117) and (118), it is possible to affirm that the structural damping can be treated as viscous damping [3] if

$$c_{eq} = \frac{\alpha}{\pi\omega} \quad (119)$$

Substituting in (36), the expression became as follow

$$m\ddot{x} + k(1 + i\eta)x = f_0 e^{i\omega t} \quad (120)$$

Where

$$\eta = \frac{\alpha}{\pi k} \quad (121)$$

Is called factor loss, and where $k(1 + i\eta)$ is defined as *complex stiffness*, whose real part represent elastic component, and imaginary part, loss stiffness [3].

The receptance is given by:

$$H(\omega) = \frac{1}{-\omega^2 m + k(1 + i\eta)} \quad (122)$$

The analogy between structural and viscous damping is valid only for harmonic excitations [2].

5.5 MOTION OF A BEAM

The case that will be studied in this research is the motion of a beam subjected to base excitation. Thus, in this section all the theoretical equations will be presented. In Figure 4.3 is shown the model that will be analysed. Only flexional modes will be considered and studied

The motion of the beam could be considered as a roto-translation motion: translation, due to the base motion, and rotation around the base constraint.

As far as reference system is concerned, $w(t)$ is the relative translation of the shaker, $y(x,t)$ is the relative translation of the beam and $z(x,t)$ is the absolute displacement. Instead, x is just the distance of a point of the beam from the constrain.

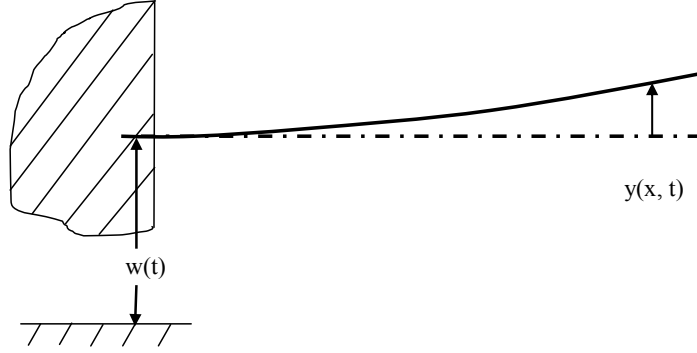


Figure 5.5 Motion of a fixed-free beam subjected to a base excitation

$$z(x, t) = w(t) + y(x, t) \quad (123)$$

The starting equation is the Eulero-Bernoulli equation [7]:

$$\mu \frac{\partial^2 z}{\partial t^2} + c \frac{\partial z}{\partial t} + EI \frac{\partial^4 z}{\partial x^4} = f(x, t) \quad (124)$$

With μ is mass per unit length

Adding (122) in (124), it follows

$$\mu \frac{\partial^2 y}{\partial t^2} + C \frac{\partial y}{\partial t} + E \frac{\partial^4 y}{\partial x^4} = -\mu' \frac{\partial^2 w}{\partial t^2} \quad (125)$$

Where, $\mu \frac{\partial^2 y}{\partial t^2}$ is the inertia of the beam, $C \frac{\partial y}{\partial t}$ is the damping, $EI \frac{\partial^4 y}{\partial x^4}$ is the stiffness of the beam and $-\mu' \frac{\partial^2 w}{\partial t^2}$ is the force excitation due to base motion.

It has been assumed that the major damping contribution comes from internal energy dissipation mechanism so we can neglect the term $C \partial w / \partial t$.

The natural frequencies and mode shapes of (74) are achieved by means of *separation of variable* approach: the displacement of a generic variable could be express as a product of a function of displacement coordinate and a function of temporal coordinate

$$y(x, t) = Y(x)\eta(t) \quad (126)$$

Starting from

$$\mu \frac{\partial^2 y}{\partial t^2} + EI \frac{\partial^4 y}{\partial x^4} = 0 \quad (127)$$

Adding (126) in (127) and solving the differential equation the expression of the *mode shapes* are obtained

$$Y_i(x) = \left\{ \frac{1}{\sqrt{\rho L}} \right\} \{ [\cosh(\beta_i x) - \cos(\beta_i x)] - D_i [\sinh(\beta_i x) - \sin(\beta_i x)] \} \quad (128)$$

Where,

$$D_i = \frac{\cos(\beta_i L) + \cosh(\beta_i L)}{\sin(\beta_i L) + \sinh(\beta_i L)} \quad (129)$$

(77) is the expression of the mass-normalized mode shapes

The eigenvalues are:

n	$\beta_n L$
1	1,875
2	4,69
3	7,85
4	10,99
5	(2n-1)

And the natural frequencies:

$$\omega_n = \beta_n^2 \sqrt{\frac{EI}{\mu}} \quad (130)$$

The displacement of the beam in function of the acceleration of the base is

$$y_n(x, \omega) = \ddot{w}(\omega) \sum_{n=1}^p \left\{ \frac{-\Lambda_n Y_n(x)}{[(\omega_n^2 - \omega^2) + j\omega_n \eta]} \right\} \quad (131)$$

with

$$\Lambda_n = \int_0^L \rho Y_n(x) dx \quad (132)$$

Defined as *modal participation factor*, that is, a vector $N \times 1$ where each terms defines the contribution of each mode to the global displacement when the system is excited in a relevant direction

6 SIMULATION & EXPERTIMENTAL TESTS

In this chapter, the experimental test and numerical model are illustrated. They were carried out in INSA Centre Val de Loire in Blois with the supervision of Professor Roger Serra.

The aim of this chapter is to show which tests were conducted and how they were performed, but overall, how the numerical model was built and which results it offers.

The logical procedures used to achieve the numerical model are shown (Figure 6.1)

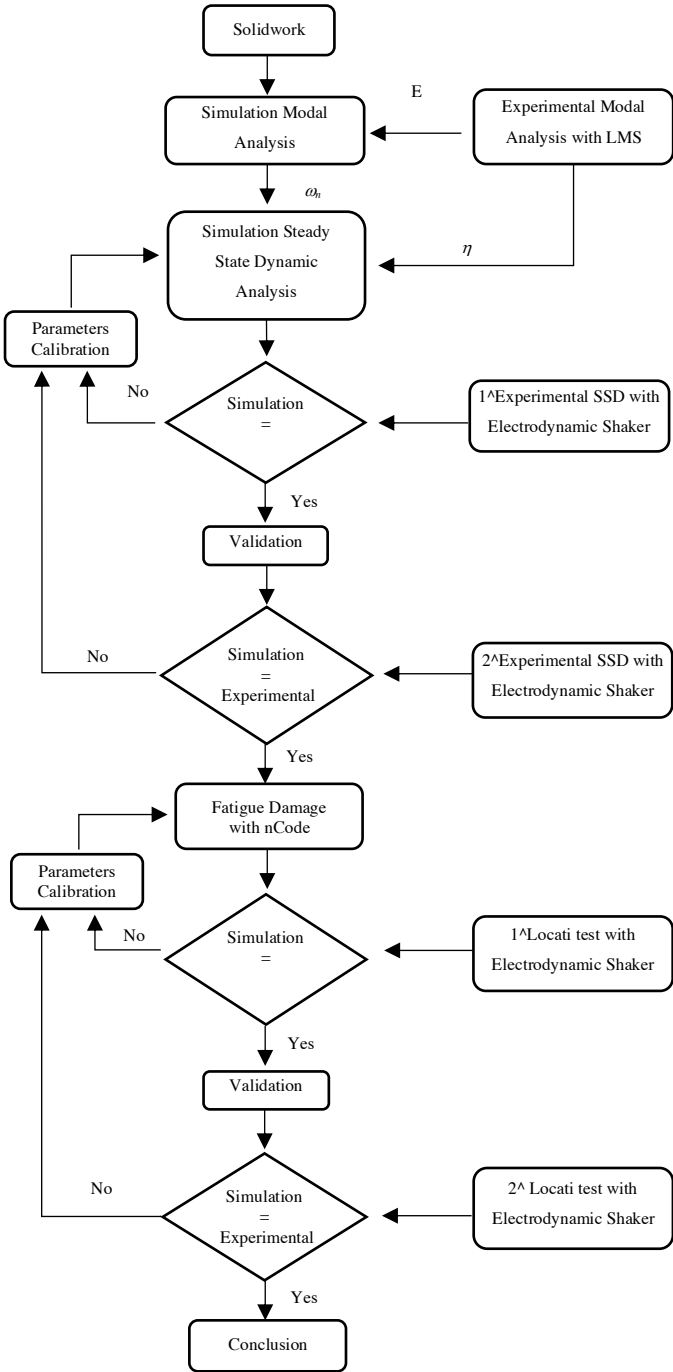


Figure 6.1 Procedures for validation of numerical simulation

6.1 SPECIMEN

The specimens used for experimental parts, identified by the names A_1 and A_2 is made of AISI 304, a common stainless steel. The specimen's geometry (Figure 6.2 and 6.3) was chosen for several motivations. The first concerns its thickness which must be small to avoid a high rigidity and long time to lead it to failure. The second is about the two notches which are stress concentration point and help to speed up the propagation of the crack. The specimens are made for breaking up in the Notch 1, highly deformed when excited in the second modal frequency and with the highest stress (Figure 6.3).

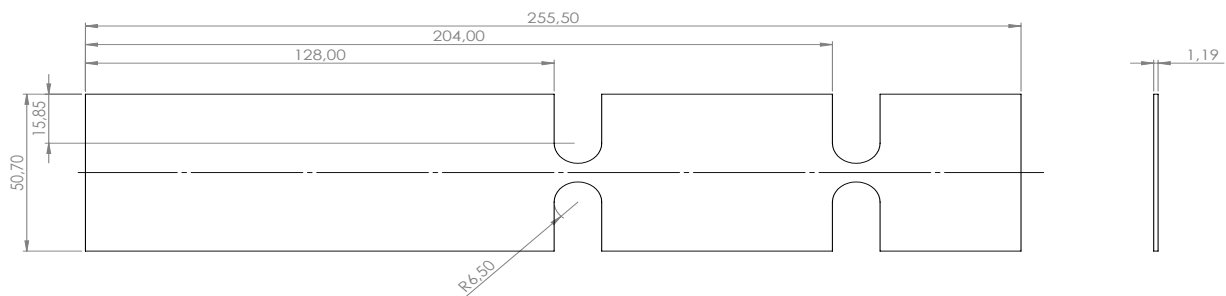


Figure 6.2 Specimen's draw

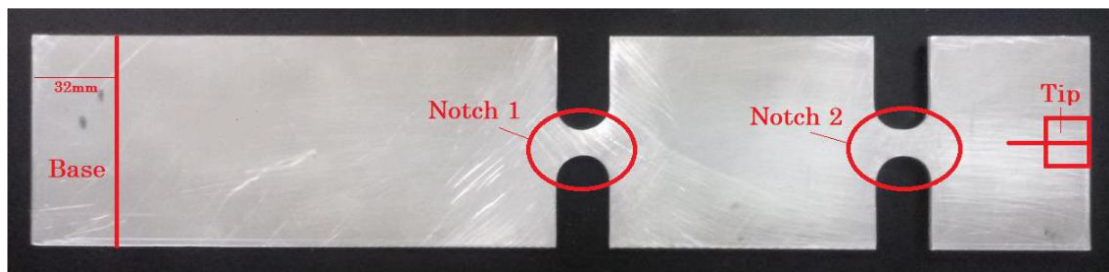


Figure 6.3 Specimen

The physical properties are reported in Table 5.1.

<i>Specification</i>	<i>Specimen A_1</i>	<i>Specimen A_2</i>
Thickness [mm]	1,19	1,19
Mass [kg]	0,1127	0,113
Volume [mm³]	14118,38	14118,38
Density [kg/m³]	7982,50	8003,75

Table 1 Specimens's physical properties

Mass and thickness have been measured experimentally, volume has been extracted by means of Solidwork and density has been obtained by the ratio between the mass and the volume

6.2 EXPERIMENTAL INSTRUMENTS

The experimental instruments used are:

- Impact hammer
- Piezoelectric Accelerometer
- Electrodynamic shaker with closed loop control system

6.2.1 Impact Hammer

The Impact Hammer (Figure 6.4) is an instrument equipped with a force sensor, made by a material, called piezoelectric, that emits an electrical charge in response to an applied stress. This charge is the output signal which provides a measurement of the amplitude and frequency content of the energy stimulus that is imparted to test object [19].



Figure 6.4 Impact Hammer

<i>Specification</i>	<i>Value</i>
Model	IH-02
Sensitivity [mV/N]	2.5
Measurement Range (Compression)	200N
Overload Capacity	120%
Temperature Range	-54 to +121 °C
Excitation Voltage	20 to 30 VDC
Constant Current Excitation	2 to 20 mA
Output Impedance	≤ 100 Ohm
Output Polarity	Positive
Hammer Head Weight	80gm
Hammer Head Diameter	16mm
Hammer Length	250mm

Table 2 Impact Hammer technical data [19]

6.2.2 Piezoelectric Accelerometer

Piezoelectric Accelerometers (Figure 6.6) are transducers that employ piezoelectric materials to measure the acceleration. Those material act as springs connecting the base of the accelerometers to a seismic mass. When accelerometer is vibrating, a force, equal to the product of the seismic mass's acceleration and seismic mass itself, is applied on the piezoelectric element. This element produces a charge proportional to the force, and as consequence to the acceleration of the seismic mass, given that the seismic mass is constant (figure 6.5).



Figure 6.6 Accelerometer

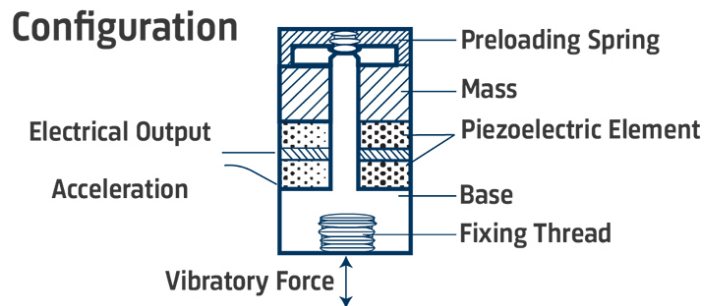


Figure 6.5 Accelerometer cross section

6.2.3 Electrodynamic shaker

The Electrodynamic shaker is extremely popular in vibration testing. It is composed by two elements: fixed and moving (Figure 6.7). The fixed part, called *exciter base*, is a permanent magnet and a field coil. Instead, the moving element, called *armature*, is the part that shift axially, transferring the move to the specimen attached to the *table*, the structure's end. The armature consists in other two parts: spider and coil. The spider is the structure that connects the armature's table with coil. The coils consist in copper wire rolled up around a nonmagnetic core made by an aluminum or magnesium thin shell. Flexures support the armature impeding any lateral or rotational motion but letting the axial motion. A cooling system is usually present for protecting the machine from an overheating

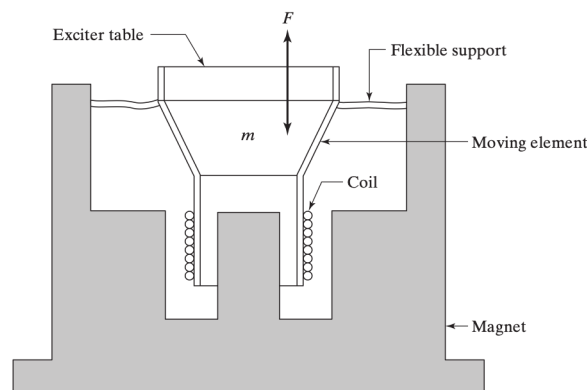


Figure 6.7 Electrodynamic shaker cross section

The operating principle of this machine is based on the Lorentz law. It receives in input a voltage and the corresponding $I(t)$ and the interaction between the electrical current and the magnetic flux of permanent magnet creates a force that allow the traslation of the armature.

The model used for the testing is *LDS V780 series* produced by Bruel & Kjaer (Figure 6.8).



Figure 6.8 Electrodynamic shaker used for testing

<i>Specification</i>	<i>Value</i>
Body Mass	381.0 kg
Sine force peak	5.12 kN
Max. random force RMS	4.23 kN
Half sine Shock Force	9.5 kN
Velocity	1.90 m/s
Max. acceleration sine peak	111 g
Max. acceleration RMS	490 m/s ²
Displacement continuous peak-peak	25.4 mm
Moving element mass	4.7 kg
Armature Resonance	2950 Hz
Usable frequency range	DC- 4 kHz
Total Heat Dissipation (from body)	3.20 kW
Total Heat Dissipation (from cooling fan)	4.8 kW
Ambient working Temperature	0-30 °C

Table 3 Shaker technical data [16]

The entire system is led by a *control system in closed loop*. The user, by means of a computer, generates an output signal which set the acceleration shaker must produce. The aim of the control system is to guarantee that acceleration signal emitted by the software coincides with the effective

shaker's acceleration and to reduce to lowest value the difference between these two signals. The control system used is *m+p International*. In Fig. 6.7 a general layout of the system is illustrated

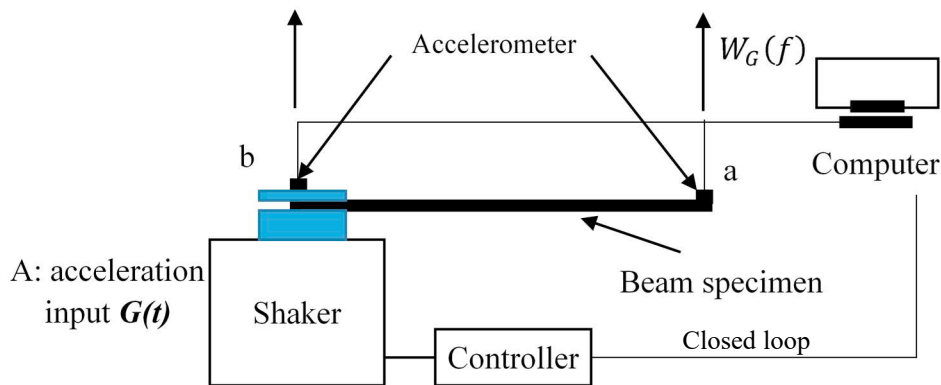


Figure 6.9 General layout of the system

6.3 EXPERIMENTAL ACTIVITY

The experimental activity is constituted by three parts:

- Experimental modal analysis (EMA) with impact test: it is a technique which provides a set of modal parameters that characterize the dynamic behaviour of a structure: natural frequencies, modal damping, and mode shapes of the specimen. The instruments used are impact hammer and accelerometer.
- Steady state dynamic (SSD) analysis (Sine test): It provides the steady-state amplitude and phase of the response of a system due to harmonic excitation at a given frequency. The instruments used are electrodynamic shaker and accelerometer.
- Fatigue cycles loads: the specimen has been subjected to random load till its failure in order to evaluate the fatigue damage. The instrumentations are the same of SSD analysis

The signals produced by electrodynamic shaker were Ergodic, Gaussian with zero mean value.

6.3.1 Experimental modal analysis

The experimental modal analysis has been conducted with the help of LMS Test.lab, a software produced by Siemens. It consists in a multichannel data acquisition system connected to the hammer and to the accelerometer. The software receives the data of the measures from the hammer and accelerometer and elaborate them with the aim of detecting the dynamic behaviour of the specimens and extracting the modal parameters.

Given that the two specimens were made of the same material and had the same geometry, only one specimen were used for the test.

To conduct the experimental tests, a numerical model that reproduce the specimen's geometry on is mandatory.

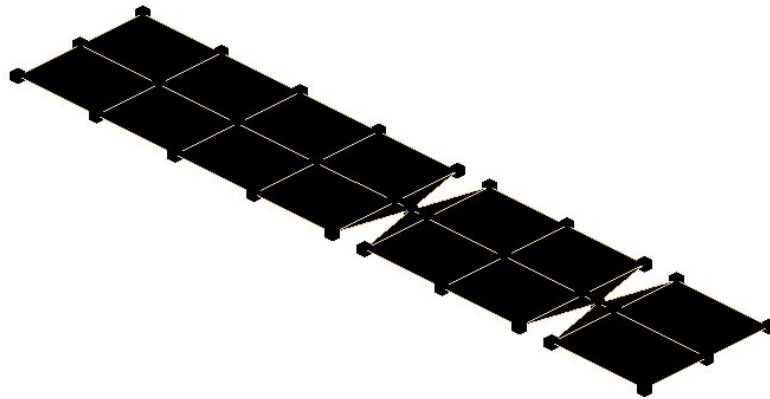


Figure 6.10 Geometry of the specimen in LMS

The interest of the research concerned just flexional oscillations, therefore, only points on the longitudinal axes were hit by the hammer

The specimens were fixed to on extremity for a length of 32mm, like a cantilever beam and the accelerometer was placed on the free extremity of the specimen (Figure 6.11).

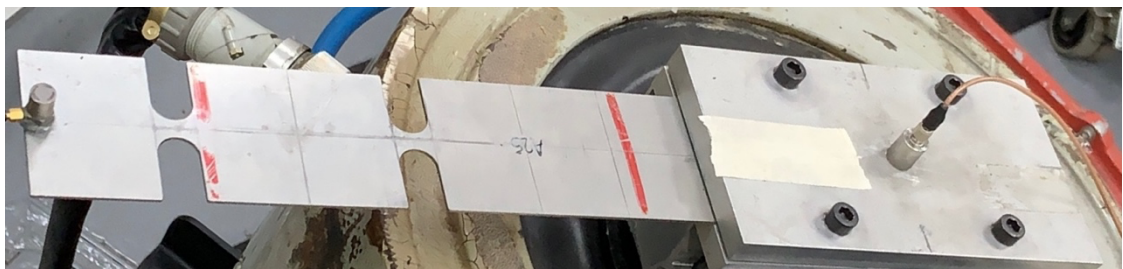


Figure 6.11 Specimen clamped according to the operative condition

The measures were executed hitting six different points with the hammer. The equivalent points on the model of those hit on the real specimen are shown in Figure 6.12.

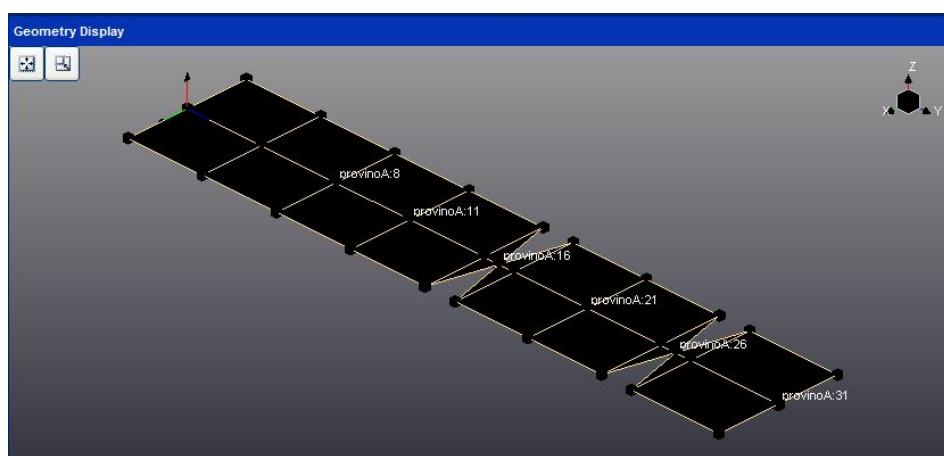


Figure 6.12 Points of the specimen hit by the hammer

For each measure, the software created an accelerated-frequency response function of the free end of the specimen (figure 6.13).

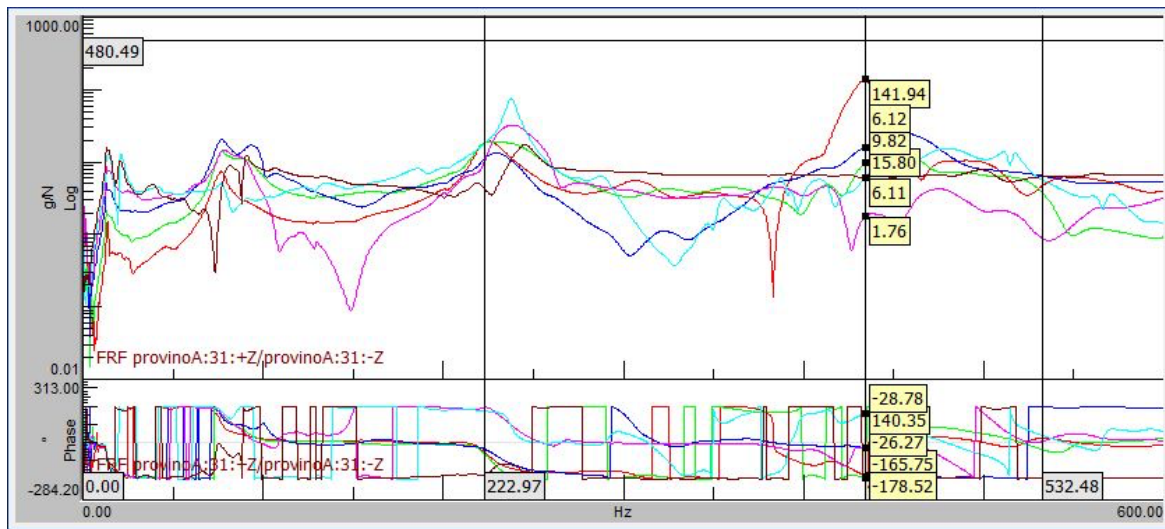


Figure 6.13 Accelerated-FRF of the measures

Successively, the analysis proceeded with the identification of modal parameters by means of *stabilization diagram*

Stabilization diagram (Figure. 6.14) is a graph where the frequencies are plotted as the x-axis and the model orders as the y-axis. The main purpose using the stabilization diagram for detecting the parameter is to distinguish physical modes from spurious modes. Spurious modes are modes that don't match with real vibration modes of the specimen, they are caused by noises or filtering mistakes from the software.

In this diagram, physical and spurious modes are represented by multiple graphical symbols.

The symbols used in LMS are f, o, s, v. Symbol 's' indicates a, so called, *stable pole*, that is equivalent to a physical mode. Instead, the other symbol represents spurious mode or, so called, *unstable pole*.

The stable poles usually appear at a nearly identical frequency, forming a vertical column, while the unstable poles tend to scatter around the frequency range.

The frequencies where the stable points form a column are usually the resonant frequencies. It could be the possibility that, in some circumstance, some columns of stable poles are placed in different frequencies from that of resonant. For choosing the right stable point, the Mode Indicator Function (MIF) is plotted (green line in Fig. 6.14).

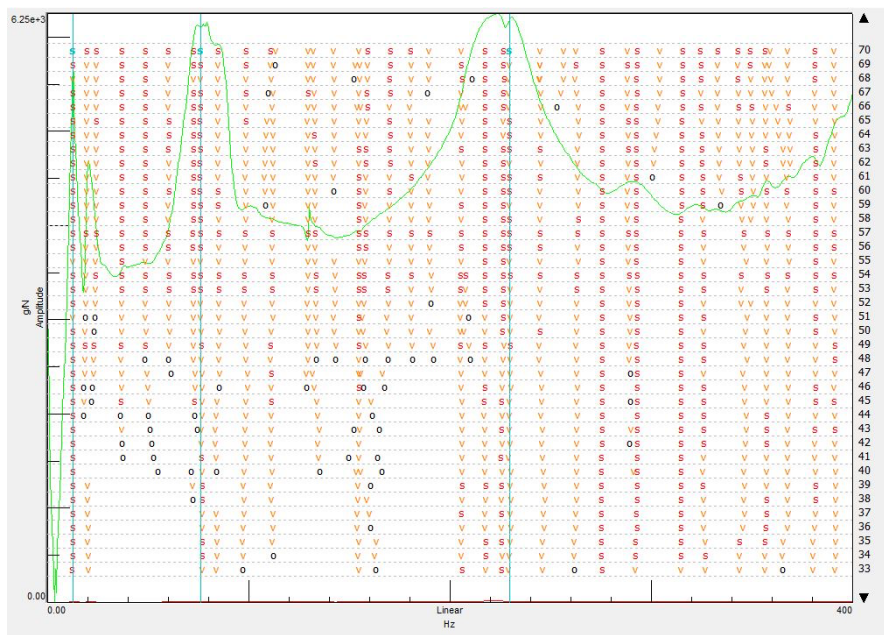


Figure 6.14 Stabilization diagram obtained for specimen A_1

The stable poles in blue are the selected ones. The poles identification required a large user experience [20], in fact for choosing the correct poles has relied on the professor's experience.

The modal parameters extracted from stabilization diagram are

<i>Mode</i>	<i>Frequency [Hz]</i>	<i>η (%)</i>
1	14,02	7,75
2	76,30	2,62
3	238,10	1,40

Table 4 Modal Parameters from EMA

The modes shapes are

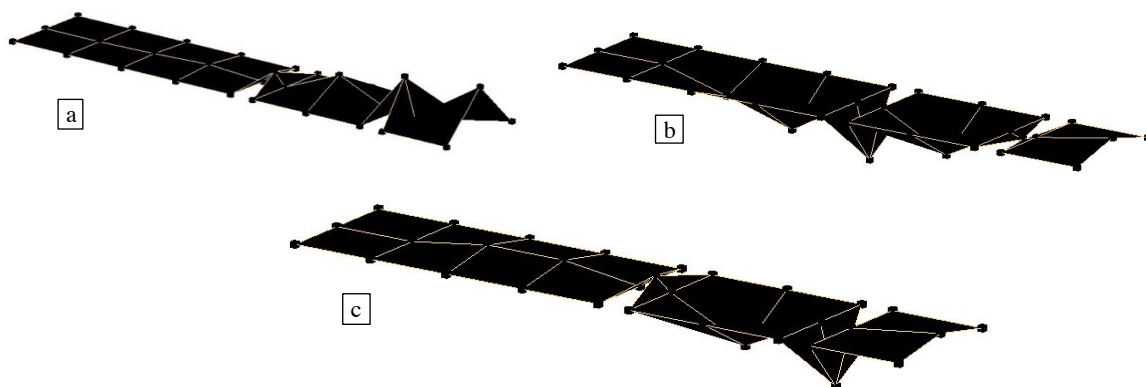


Figure 6.15 Flexional mode shapes : a) first mode, b) second mode, c) third mode

6.3.2 Steady State Dynamic Analysis – Sine test

Steady-state dynamic analysis, or Sine test, consists in the measure of the amplitude and phase of the response of a system due to harmonic excitation at a given frequency, also called, Frequency Response Function (Chapter 5.3). Usually, such analysis is a frequency sweep where a force at a constant amplitude in a frequency range is applied and the response is recorded. The response can be measured as displacement, velocity or acceleration.

The analysis has been conducted with the help of an electrodynamic shaker. The specimen has been clamped on the top of the shaker for a length of 32cm and the accelerometer has been placed on the free end of the specimen (Figure 6.16 e 6.17). The frequency range chose for the analysis is 10-300Hz and the amplitude of the load is given in terms of acceleration, 1g.

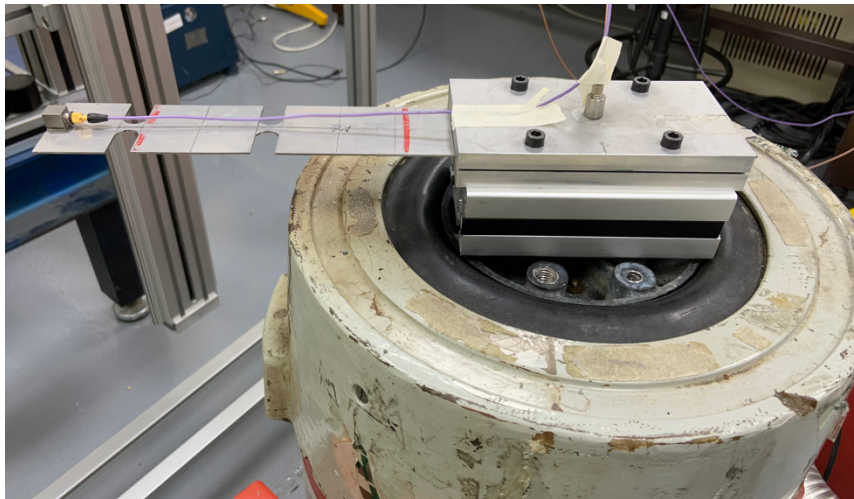


Figure 6.17 Experimental setup

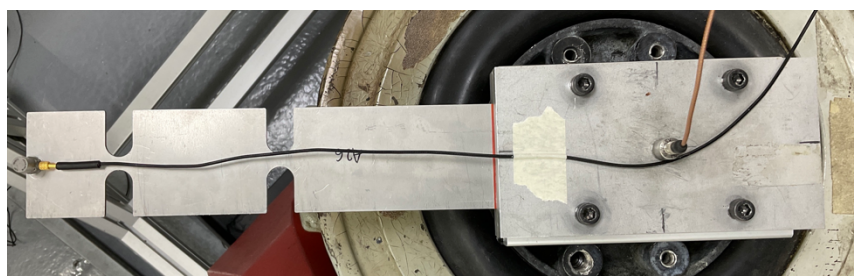


Figure 6.16 Experimental setup (top view)

In Figure 6.18, it is shown the computer's display after the sine test. In the top, there is the acceleration that shaker produced in input, in the middle, the error between the effective shaker's acceleration produced and the target acceleration it should have produced, while in the bottom the specimen's free end acceleration in frequency range.

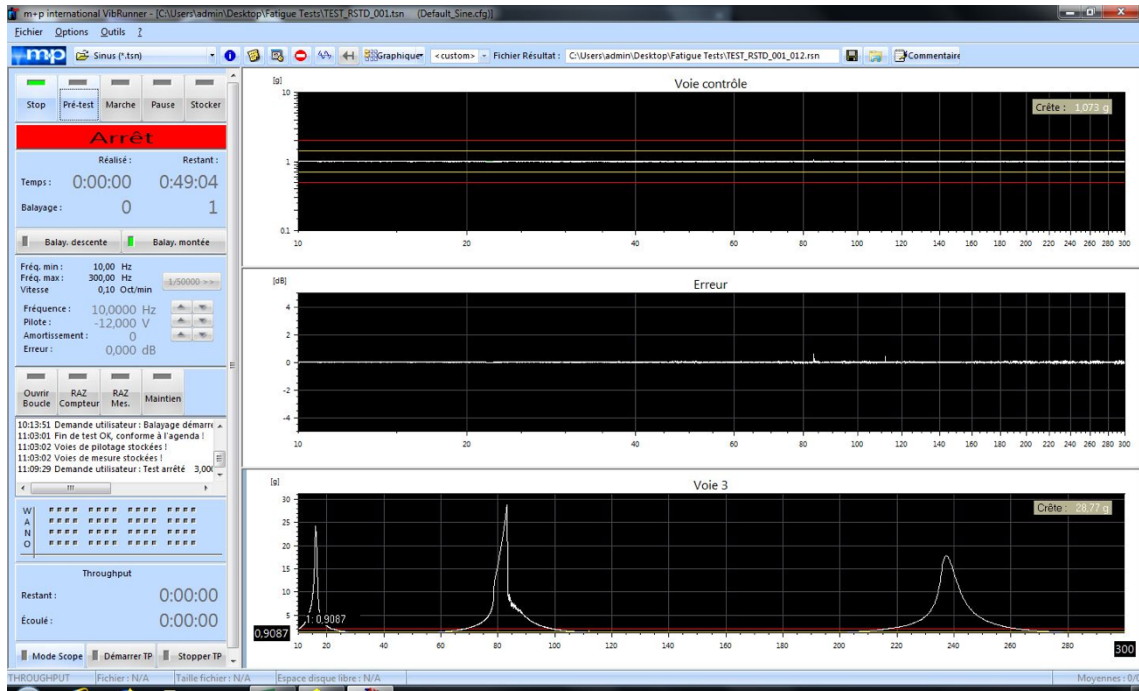


Figure 6.18 Sine test: input acceleration (top), error between output acceleration and input acceleration (middle), acceleration of specimen's free end (bottom)

In figure 6.19, the free end acceleration for both specimens are shown. In table 4 the value of the amplitude and frequency of the peak of accelerated FRF are shown.

<i>Specimen</i>	<i>Frequency [Hz]</i>	<i>Δf (Exp-LMS)</i>	<i>Relative Error to</i>	<i>Amplitude [g]</i>
		<i>[Hz]</i>	<i>LMS (%)</i>	
A_25	15,89	1,87	13,3	24,49
	81,54	5,24	6,9	27,07
	232,043	6,057	2,5	15,92
A_26	16,09	2	14,3	24,20
	83,28	6,98	9,2	28,77
	237,16	5,12	2,2	17,85

Table 5: Amplitude and Frequency of the Accelerated FRF

It could note that the resonant frequencies obtained with sine test are quite different from those extracted from EMA. The explanation of that difference could be found in the application of the load (impact and random excitation).

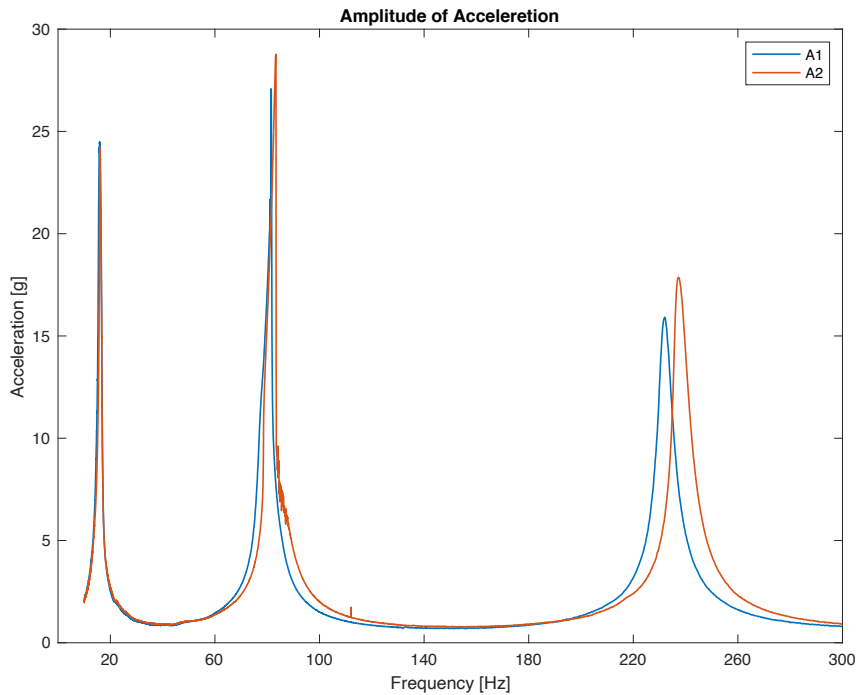


Figure 6.19 Experimental accelerated-FRF

6.3.3 Fatigue cycles loads

The last experimental part was the fatigue cycle tests. The instrumentation is the same of the previous analysis: electrodynamic shaker and accelerometer. For analyzing the fatigue damage, Locati method has been used. This method was proposed by L. Locati in 1955 with the aim of accelerating fatigue experiments. A step load instead of a constant load is used, this should reduce the test time and the number of test pieces required too. The specimen is loaded, for fixed time interval, by an initial stress value which should not exceed the lowest expected value of fatigue limit [14]. After that time interval, the load is increased of a fixed increment till the specimen has a failure.

In this analysis, the load is expressed in terms of Power Spectral Density (PSD) in $[g^2/Hz]$. The fixed time interval is 1h, the initial load is $0,25 g^2/Hz$ and the fixed increment are $0,05 g^2/Hz$.

The specimen A_1 had a failure after 10h42min with a PSD of $0,75 g^2/Hz$ (Figure 6.20). Instead, the specimen A_2 had a failure after 11h14min with a PSD of $0,8 g^2/Hz$ (Figure 6.21). The amplitude of frequency range was 80 Hz centered on the second frequencies obtained in SSD analysis: for specimen A_1, 41-121 Hz while for specimen A_2, 43-123. The decision to have a frequency range centered in the second frequency is dictated by the intention of working with a wide frequency band. In the case it had worked around the first frequency the band would have not been so wide, because it is too close to 0Hz, and the amplitude would have not been higher than 20Hz.

In addition to PSD , the value of equivalent acceleration expressed in $[g]$ (g_{RMS}) for all the level of load is given by:

$$gRMS = \sqrt{PSD * \Delta f}$$

Test	PSD [g²/Hz]	RMS [g]	Time [s]
1	0,25	4,472	3600
2	0,3	4,899	3600
3	0,35	5,292	3600
4	0,4	5,657	3600
5	0,45	6,000	3600
6	0,5	6,325	3600
7	0,55	6,633	3600
8	0,6	6,928	3600
9	0,65	7,211	3600
10	0,7	7,483	3600
11	0,75	7,746	2520

Table 6 PSD Load and gRMS for specimen A_1

Test	PSD [g²/Hz]	RMS [g]	Time [s]
1	0,25	4,472	3600
2	0,3	4,899	3600
3	0,35	5,292	3600
4	0,4	5,657	3600
5	0,45	6,000	3600
6	0,5	6,325	3600
7	0,55	6,633	3600
8	0,6	6,928	3600
9	0,65	7,211	3600
10	0,7	7,483	3600
11	0,75	7,746	3600
12	0,8	8	876

Table 7 PSD Load and gRMS for specimen A_2

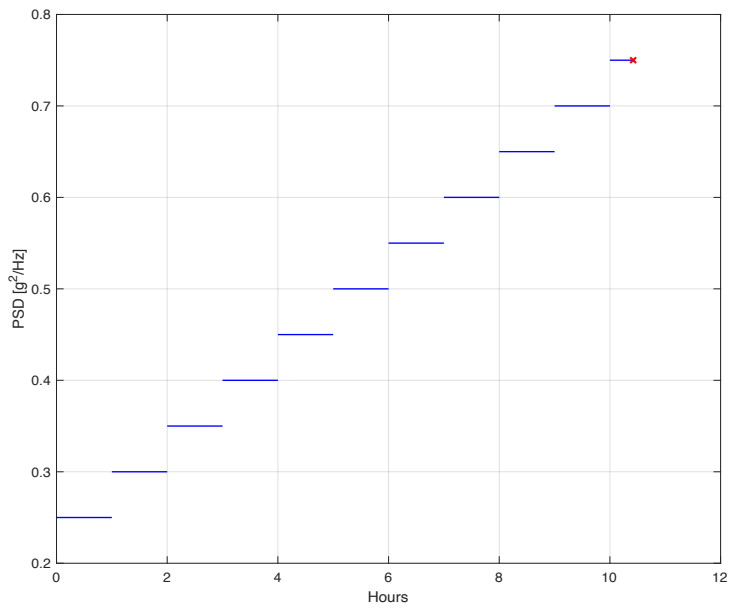


Figure 6.20 Cycle Load for specimen A1

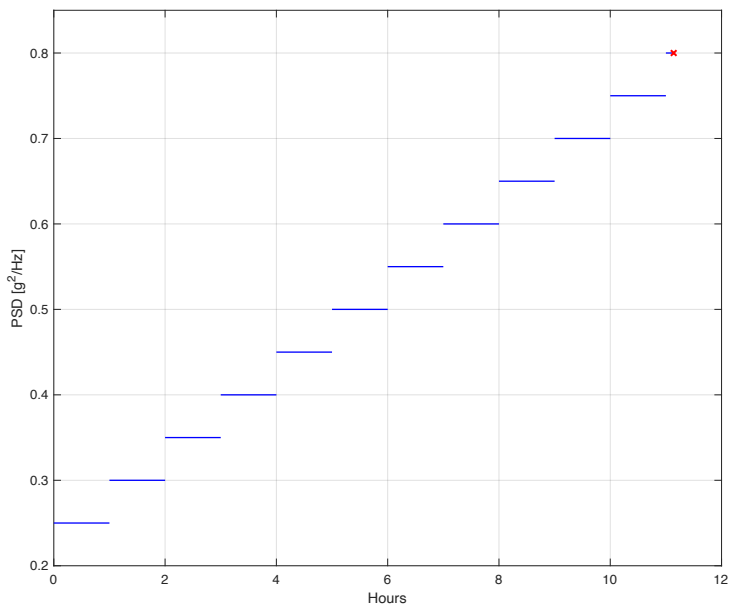


Figure 6.21 Cycle Load for specimen A2

The fatigue failure for the two specimens occurs in the notch 1, because it is the most deformed and most stressed point in the structure when the frequency is close to second resonant (Figure 6.22).

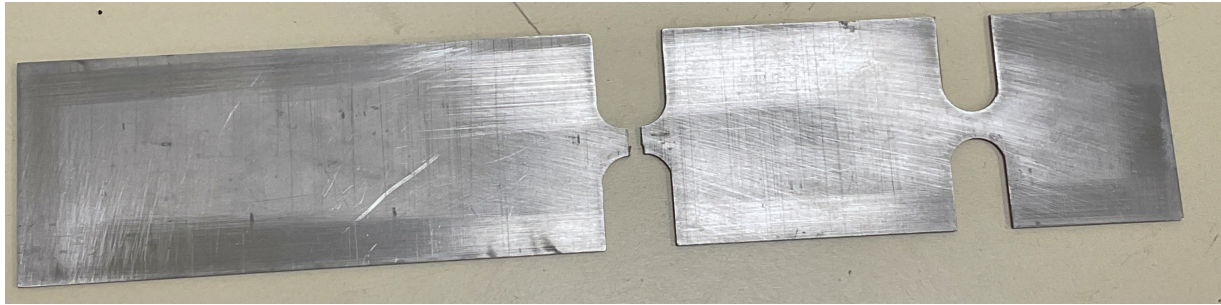


Figure 6.22 Specimen failed

6.4 NUMERICAL SIMULATIONS

All the experimental analysis were reproduced with numerical simulation by means of two software: ABAQUS and nCode with the purpose of recreating a precise model of the specimens to analyze the fatigue damage

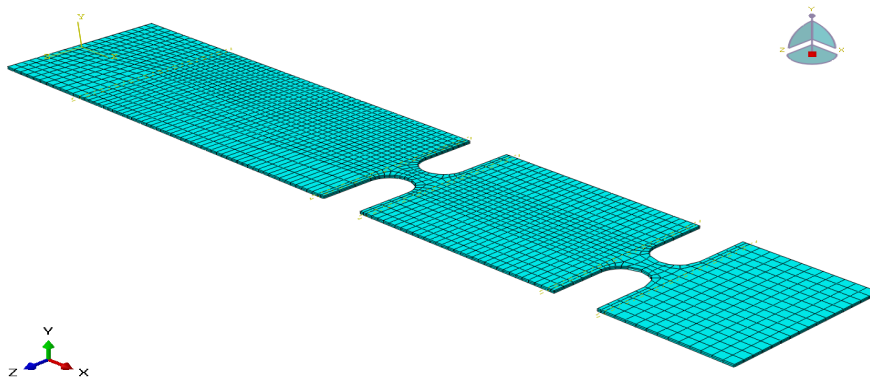


Figure 6.22 Mesh of the model

6.4.1 Numerical Modal Analysis

The numerical modal analysis has been implemented with ABAQUS.

The first step of the analysis was to create the mesh of the model (Figure 6.22). The mesh was made of 4408 hexagonal elements.

For carrying out the analysis, the software required the mass density value and the Young' module value (E). The first one is obtained by the average of the mass value of the two specimens (112,9 kg), instead, as far as the second one is concerned, an iteration has been required. The value of first attempt has been extracted from the natural frequencies obtained from EMA (Table 4) with the expression

$$E = \frac{\omega_n^2 \mu}{\beta_n^4 I}$$

The frequencies resonant extracted from EMA were considered a little more reliable than those obtained from shaker, because they could be affected by a non-perfect clamping.

Afterward, the value of E has been updated to obtain from simulation natural frequencies values close to experimental value. The final value of E was 190MPa.

As far as boundary condition is concerned, one of the extremities of the model were constrained for a length of 32 mm (Figure 6.23), preventing any translations or rotations.

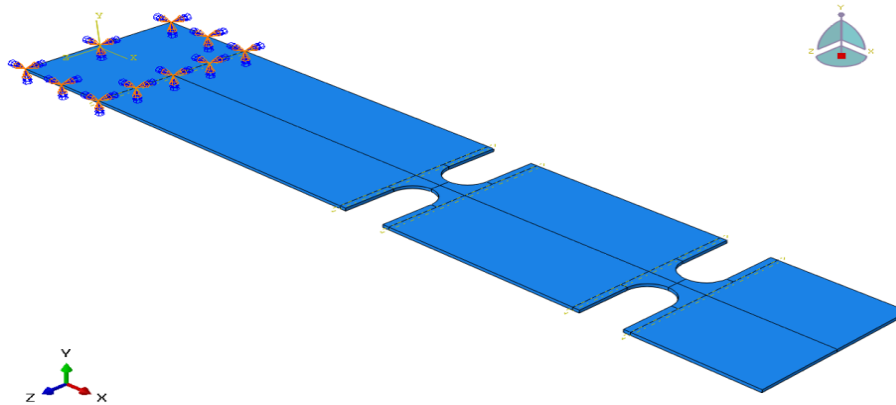


Figure 6.23 Boundary condition of the model

Successively, the natural frequencies, the participation factor, the effective mass that contribute to the single vibration mode (Table 8), and the firsts three flexional modes shapes (Figure 6.24 a, b, and c) were extracted.

<i>Mode</i>	<i>Frequency [Hz]</i>	<i>Participation factor</i>	<i>Effective Mass</i>
1	15,5	0,046	2,11E-03
2	82,9	0,013	1,80E-04
3	224,2	0,005	2,48E-05

Table 8 Natural Frequencies, participation factor, and effective mass from numerical simulation

The relative errors between the numerical natural frequencies and the experimental ones are shown in Table 9.

<i>Mode</i>	<i>Δf (Sim- LMS) [Hz]</i>	<i>Relative error to LMS (%)</i>	<i>Δf (Sim- A25) [Hz]</i>	<i>Relative error to A_25 (%)</i>	<i>Δf (Sim- A26) [Hz]</i>	<i>Relative error to A_26 (%)</i>
1	1,5	10,5	0,3	2,5	0,6	3,7
2	6,6	8,71	1,4	1,8	0,4	0,3
3	13,9	5,8	7,8	3,3	13	5,4

Table 9 Comparison between numerical and experimental results

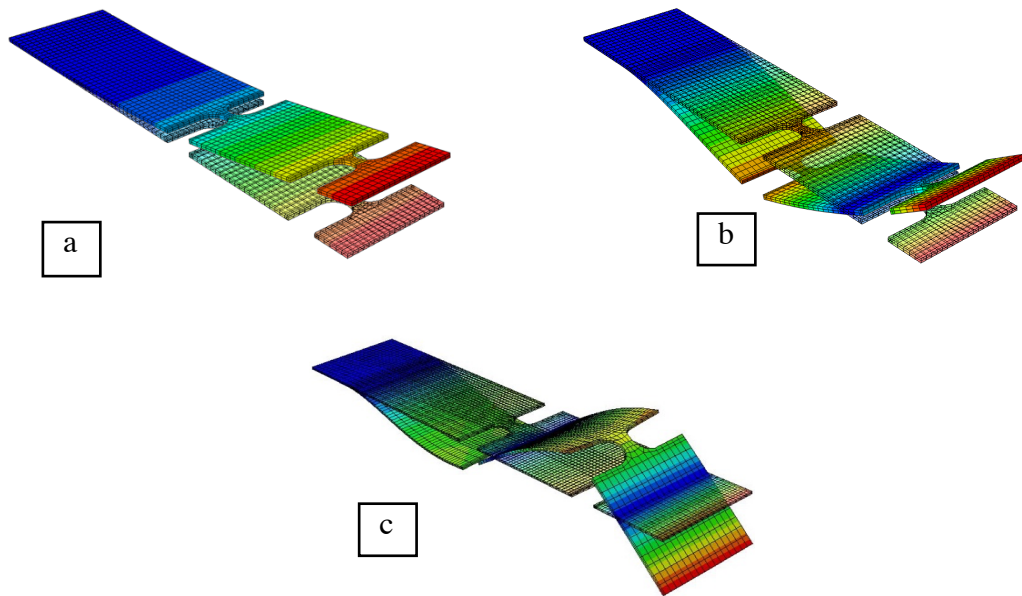


Figure 6.24 a) 1st flexion mode, b) 2nd flexion mode, c) 3rd flexion mode.

In table 8, it is possible to note that the flexional mode 1 has the highest participation factor between the three modes and the highest effective mass. It means that the first mode participates more than the other modes in the global motion of the specimen but overall, it involves more mass than the others.

6.4.2 Numerical Steady State Dynamic

In Abaqus such analysis is based on modal superposition technique, considering the modes extracted in the step before. The frequency range considered is 0-300 Hz.

As far as modal damping is concerned, it has been decided to select a structural damping, considered as the most precise. As it happened for Young's module, an iteration for obtaining correct values of modal damping has been performed. The first attempt values were those obtained in EMA (Table 4). Later, thanks to the experimental value, modal damping values were calibrated and validated, obtaining the following results

<i>Mode</i>	<i>η (%)</i>
1	6,8
2	3,1
3	3

Table 10 Damping Value Updated

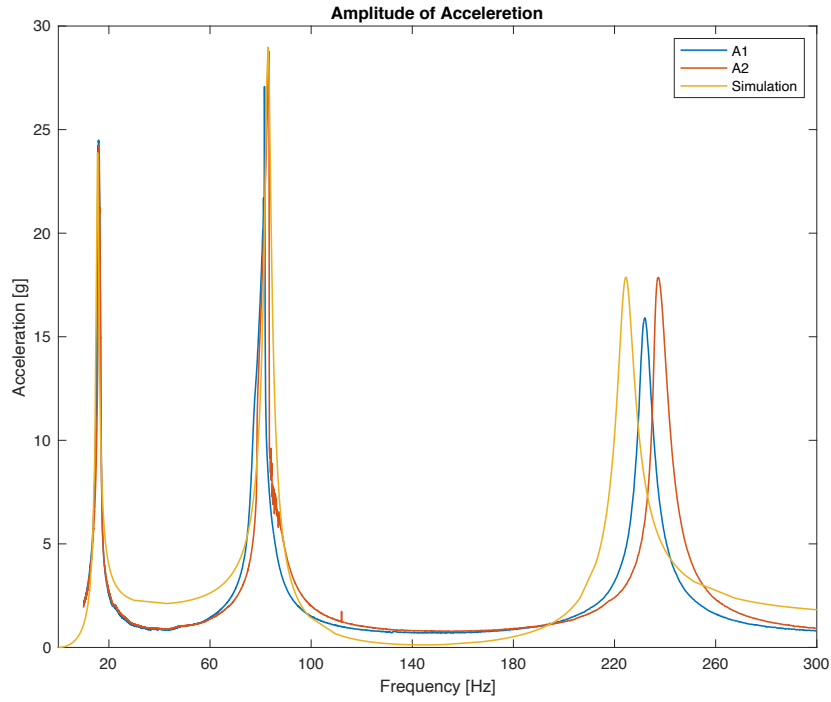


Figure 6.25 Acceleration of free end: simulation vs experimental

The amplitude of the harmonic oscillation, corresponding to 9,81 m/s. In figure 6.25, the acceleration of specimen's free end is shown

In Table 10 the value of the amplitude and the frequency of the peaks are illustrated

The simulated acceleration results to be very close to those gathered experimentally, especially in the first and second resonant. The displacement of specimen's free end and the stress distribution are shown in figure 6.24 and figure 6.25

<i>Mode</i>	<i>Frequency [Hz]</i>	<i>Amplitude [g]</i>
1	15,4924	23,8738
2	82,945	28,9776
3	224,505	17,873

Table 11 Amplitudes and frequencies

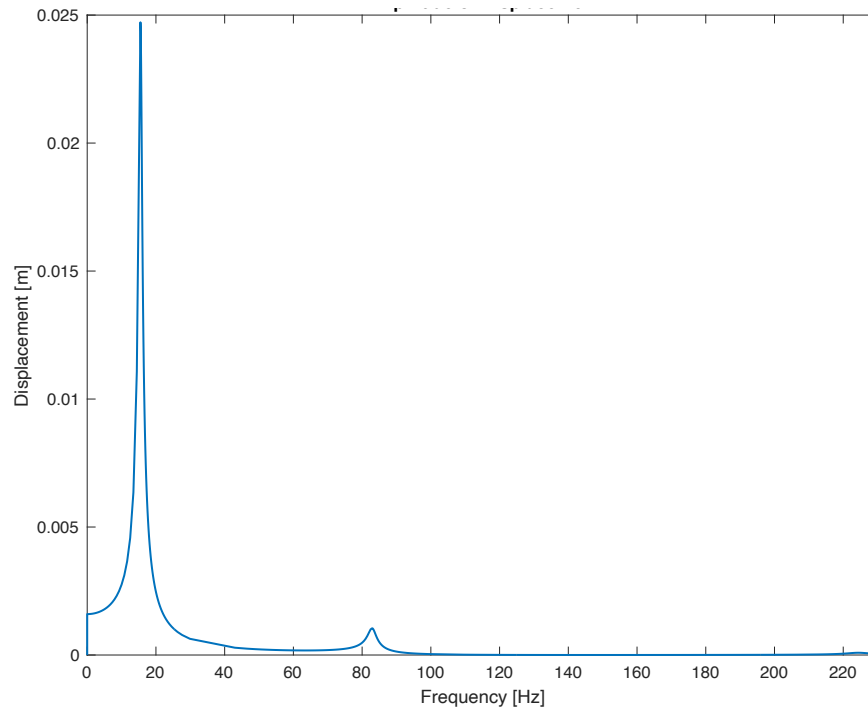


Figure 6.26 Displacement of the free end

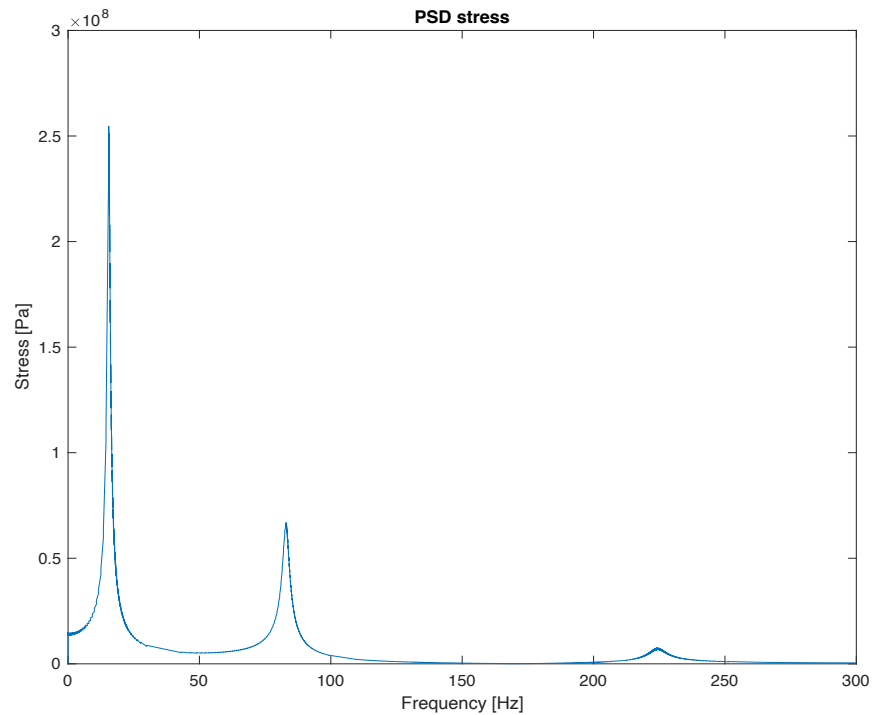


Figure 6.27 Stress distribution in Notch 1 in frequency range

Unlike the acceleration and displacement, the stress distribution was obtained from the notch 1 (Figure 6.28 & 6.29), considered as the most stressful zone in the specimen and where the failure occurs.

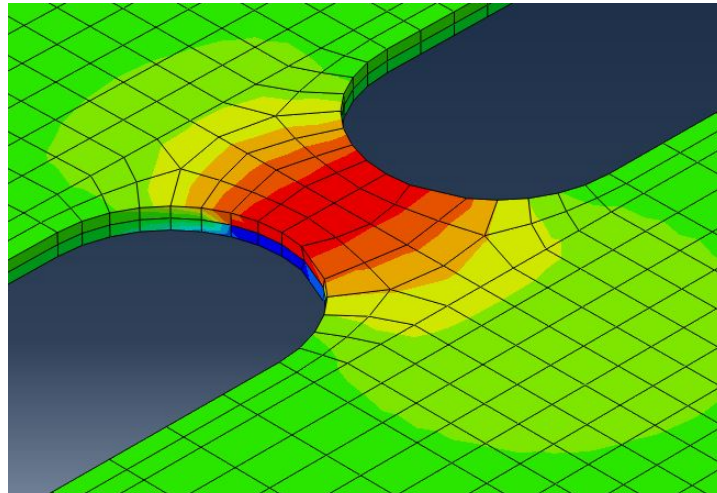


Figure 6.28 Stress distribution on notch 1

To conclude, the ABAQUS model reveals to be very accurate and very representative of the real behavior of the specimen. Thus, it has been validated and it has been possible to continue the numerical analysis.

6.4.3 Numerical Fatigue cycles loads

The fatigue cycle loads numerical simulation is carried out by the software nCode DesignLife. This software contains several sets of solvers and advanced methods for predicting structural durability and for calculating realistic fatigue lives from finite element analysis (FEA) result files.

In this research, it was used for reproducing in numerical terms the effect of the experimental loads.

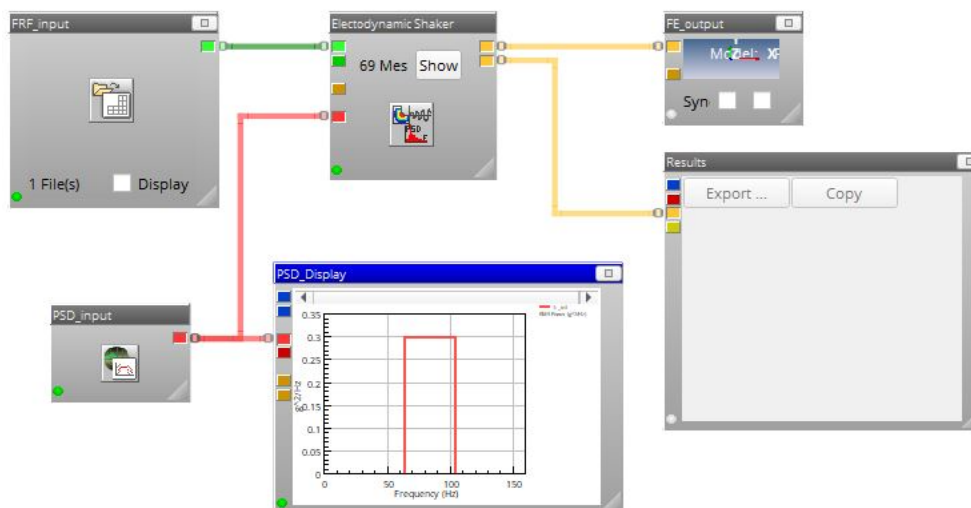


Figure 6.29 Ncode Display

In figure 6.30 it shown the interface of the software. As it shown, for carrying out the analysis, a series of boxes are connected between them by means of lines. The boxes from which the lines start

containing the information in input (FRF_input and PSD_input), those where the lines finish contain the information in output (FE_output and Results) while the only box, where the line start and finish, is the one which enable the fatigue calculation to be carried out to simulate vibration testing (Electrodynamic shaker).

The input nCode require are the FRF results file obtained from ABAQUS (FRF_input) and the value of PSD (PSD_input).

The informations in output provide the fatigue damage produced by each cycle (Table 12 & 13) and the display of stress distribution in the specimen (Figure 6.31)

It has been necessary to run as many simulations as the number of load steps. Considering that the specimen A_25 failed at 0,75 g²/Hz but specimen A_26 failed at 0,8 g²/Hz, the simulation at load level at 0,75 g²/Hz has been done twice, one at time duration of 2520 s and the second for 3600s

The results of the numerical simulation about the two specimens are illustrated in table ()

<i>Test</i>	<i>PSD [g²/Hz]</i>	<i>gRMS [g]</i>	<i>Damage</i>	<i>RMS Stress [Pa]</i>	<i>Time [s]</i>
1	0,25	4,472	0,0077	6,85E+07	3600
2	0,3	4,899	0,0164	7,51E+07	3600
3	0,35	5,292	0,0292	8,11E+07	3600
4	0,4	5,657	0,0465	8,66E+07	3600
5	0,45	6,000	0,0684	9,19E+07	3600
6	0,5	6,325	0,0951	9,69E+07	3600
7	0,55	6,633	0,1269	1,02E+07	3600
8	0,6	6,928	0,1635	1,06E+08	3600
9	0,65	7,211	0,2055	1,11E+08	3600
10	0,7	7,483	0,2528	1,14E+08	3600
11	0,75	7,746	0,1269	1,02E+08	2520
Total			1,14		

Table 12 Simulation results of Locati test of specimen A1

<i>Test</i>	<i>PSD [g²/Hz]</i>	<i>gRMS [g]</i>	<i>Damage</i>	<i>RMS Stress [Pa]</i>	<i>Time [s]</i>
1	0,25	4,472	0,0077	6,85E+07	3600
2	0,3	4,899	0,0164	7,51E+07	3600
3	0,35	5,292	0,0292	8,11E+07	3600
4	0,4	5,657	0,0465	8,66E+07	3600
5	0,45	6,000	0,0684	9,19E+07	3600

6	0,5	6,325	0,0952	9,69E+07	3600
7	0,55	6,633	0,1269	1,02E+07	3600
8	0,6	6,928	0,1635	1,06E+08	3600
9	0,65	7,211	0,2055	1,11E+08	3600
10	0,7	7,483	0,2528	1,14E+08	3600
11	0,75	7,746	0,3057	1,19E+08	3600
12	0,8	8	0,0886	9,51E+07	876
Total			1,40		

Table 13 Simulation results of Locati test of specimen A2

The stress distribution after a single fatigue cycle load in the specimen is shown in Figure 6.31

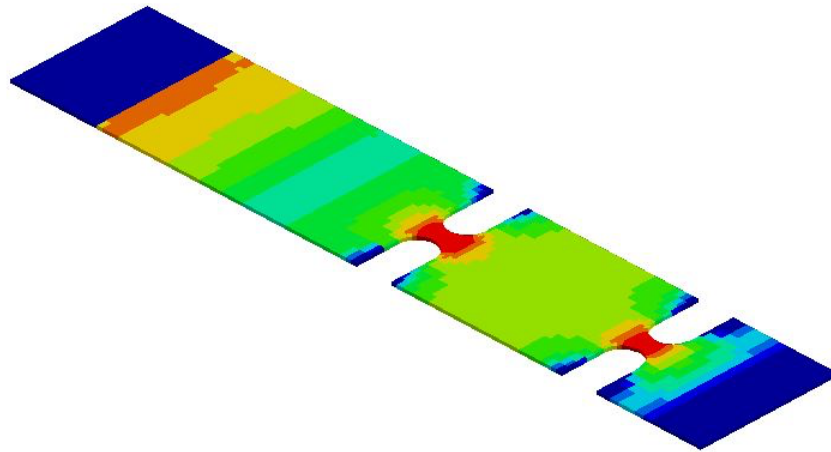


Figure 6.30 Stress distribution in nCode

For computing the total fatigue damage, the linear damage accumulation method, according to Palmgreen and Miner's rule, has been used.

As it can see in the two table, the total fatigue damage after the failure for both the specimen results to be slightly bigger than one. In fact, as said previously, the Palmgreen and miner's rule is just an approximation. It has been demonstrated that not always a material has a failure when the critical damage is equal to one. In fact, this method doesn't consider the order of the loads. If the load starts from low level, and later it increases, it could be possible that the failure occurs when the damage is bigger than 1 [4].

Therefore, it could conclude by stating that the model reproduces with reliable accuracy the fatigue behavior of the specimen.

7 CONCLUSION

To summarize, in this research it has been observed that Random vibrations are a dangerous phenomenon. In these cases, instantaneous vibration amplitudes are not highly predictable as the amplitude at any point in time is not related to that at any other point in time.

The unpredictable behavior makes difficult to calculate the useful life and the design of the component. Predicting fatigue life under random vibration loads is critical requirement.

The use of the method proposed in literature could be a good practice, but considering that they offer just an approximated result, they don't appear to be so accurate as required.

Conducting as many tests as possible could offer a valid solution, but it could result to be very expensive, and it could require long time.

Numerical simulation appears to be a good way for solving the critical problem.

In this research, a numerical model for calculating fatigue damage has been proposed. The results obtained seem to be very accurate and close to experimental values. They give a good representation of the resonates frequencies mode shape, and modal damping. The estimation of the fatigue result using the linear accumulation theory appear to be representative of experimental evidence.

This model, purposely, takes into consideration just the uniaxial case. As further step, it could be interesting to extend this model to multiaxial case as well or to add the analysis of the crack propagation.

6 REFERENCE

- [1] Bendat J.S., Piersol A.G., *Random Data: Analysis and Measurement Procedures*, Wiley & Sons, inc., New York, 1986
- [2] Meirotovich L., *Elements of Vibration Analysis*, McGraw-Hill, New York, 1986
- [3] A. Fasana, S. Marchesiello, *Meccanica delle vibrazioni*, Torino, CLUT, 2006
- [4] Milella Pietro Paolo, *Fatigue and corrosion in metals*, Milano, Springer, 2013
- [5] J. Rösler, H. Harders, M. Bäker, *Mechanical Behaviour of Engineering Materials*, Springer, 2007
- [6] Irvine T., *Spectral moment notes*, Vibrationdata, 2015
- [7] Kenneth McConnell, *Vibration Testing: theory and practice*, Wiley & Sons, inc., New York, 1997
- [8] N.M.M. Maia, J.M.M. Silva, *Theoretical and experimental Modal Analysis*, Wiley & Sons, inc., New York, 1997
- [9] Genta Giancarlo, *Vibration Dynamics and Control*, Springer, 2009
- [10] Irvine T., *Shock and vibration stress as a function of velocity*, Vibrationdata, 2013
- [11] D.Benasciutti, R.Tovo, *Comparison of spectral methods for fatigue analysis of broad-band Gaussian random processes*, Probabilistic Engineering Mechanics 21 (2006) 287–299
- [12] Matjaž Mršnik, Janko Slavic and Miha Boltežar, *Frequency-domain methods for a vibration-fatigue-life estimation - Application to real data*, International Journal of Fatigue, Vol. 47, p. 8-17, 2013.
- [13] Quigley, J., Lee, Y., and Wang, L., *Review and Assessment of Frequency-Based Fatigue Damage Models*, SAE Int. J. Mater. Manf. 9(3):2016, doi:10.4271/2016-01-0369.
- [14] Yuzhu Wang, Roger Serra et Pierre Argoul, *Adapted Locati method used for accelerated fatigue test under random vibrations*, Procedia Structural Integrity 19 (2019) 674–681
- [15] Curtis E. Larsen, Tom Irvine, *A review of spectral methods for variable amplitude fatigue prediction and new results*, Procedia Engineering 101 (2015) 243 – 250
- [16] <https://www.bksv.com/-/media/literature/Product-Data/bu3104.ashx>
- [17] Irvine T., *An introduction to frequency response functions*, Vibrationdata, 2000
- [18] A.Carpinteri, A. Spangoli and S.Vantadori, *A review of multiaxial fatigue criteria for random variable amplitude loads*, Fatigue & Fracture of Engineering Materials & Structures, 2017.
- [19] www.djbinstruments.com/products/instrumentation/impact-hammers/view/ih-02

- [20] J.Lau, J.Lanslots, B.Peeters, H.Van der Auweraer, *Automatic modal analysis: reality or myth?*, Sound & Vibration · January 2007
- [21] Wirsching P.H., Light M.C., *Fatigue under wide band random stresses*, J. Struct. Div., ASCE, 106(7), p. 1593-1607, 1980.
- [22] Ortiz, K. and Chen, N.K. *Fatigue Damage Prediction for Stationary Wide-Band Stresses* presented at the 5th International Conference on the Applications of Statistics and Probability in Civil Engineering, Vancouver, Canada, 1987.
- [23] Dirlik T. *Application of Computers in Fatigue Analysis*. PhD thesis, The University of Warwick, 1985.
- [24] Zhao W. and Baker M. J. *On the probability density function of rainflow stress range for stationary gaussian processes*. Int. J. Fatigue, 14(2):121– 135, March 1992.
- [25] Lalanne, C., *Mechanical Vibration and Shock*, Vol. 3, 4 and 5, Hermes Penton Science, London, 2009.
- [26] Benasciutti D. and Tovo R. *Spectral methods for lifetime prediction under wide-band stationary random processes*. Int. J. Fatigue, 27(8):867–877, 2005.
- [27] Larsen C., Lutes L., *Predicting the Fatigue Life of Offshore Structures by the Single-Moment Spectral Method*, Probabilistic Engineering Mechanics, 6(2), 1991
- [28] M. Matsuishi and T. Endo, *Fatigue of metals subject to varying stress*, Paper presented to Japan Society of Mechanical Engineers, Fukuoka, Japan, 1968.
- [29] MA Miner, *Cumulative damage in fatigue*, J. Appl. Mech., 12: A159–A164, 1945.